Received 25 June 2023; revised 3 August 2023; accepted 20 August 2023. Date of publication 29 August 2023; date of current version 19 September 2023.

Digital Object Identifier 10.1109/OJCOMS.2023.3309758

Short-Packet Communication Over a Two-User Rayleigh Fading Z-Interference Channel: From Stability Region to the Age of Information

J. DEERAJ KUMAR[1], PARTHAJIT MOHAPATRA[1] (Member, IEEE), AND NIKOLAOS PAPPAS[2] (Senior Member, IEEE)

[1]Department of Electrical Engineering, Indian Institute of Technology Tirupati, Tirupati 517619, India

[2]Department of Computer and Information Science, Linköping University, 581 83 Linköping, Sweden

CORRESPONDING AUTHOR: P. MOHAPATRA (e-mail: parthajit.mohapatra@gmail.com)

The work of J. Deeraj Kumar and Parthajit Mohapatra was supported by the Indo-Sweden Project, Department of Science and Technology (DST), India. The work of Nikolaos Pappas was supported in part by the Swedish Research Council (VR), ELLIIT, Zenith, and in part by the European Union (ETHER) under Grant 101096526. Short version of the work has been published in IEEE Globecom Conference [1] [DOI: 10.1109/GLOBECOM48099.2022.10001007].

ABSTRACT One of the fundamental challenges in 5G and beyond technologies is to support short packet transmissions while ensuring ultra-reliable communication. Due to the distributed nature of the networks, such as machine-to-machine (M2M) communications, interference is unavoidable. The impact of interference on the system's performance must be better understood when users are constrained to transmit short packets. In addition, users' traffic is bursty. Thus, they may not always have data to send. This work considers a two-user Z-interference channel (Z-IC) under Rayleigh fading. The work characterizes the stability region corresponding to prominent interference mitigation schemes such as treating interference as noise, successive interference cancellation, and joint decoding schemes using the finite block-length information theory framework. The developed results consider the packet length, rate, and underlying channel model. Evaluating stability region involves determining the probability of successful decoding for the various interference mitigation techniques. The different probabilities of successful decoding are characterized for various interference mitigation techniques. These results are not explored in the existing literature in the context of Z-IC. The developed results also help to explore the impact of interference on average delay and the average age of information for various interference mitigation techniques.

INDEX TERMS Finite block-length coding, Z-interference channel, average throughput, stability region, average delay, average age of information.

I. INTRODUCTION

SHORT packet communication is considered to be a key enabler in supporting two essential application scenarios of 5G, namely: (a) massive machine type communication (mMTC) and (b) ultra-reliable low-latency communication (uRLLC). Many existing performance metrics, such as capacity and outage probability, cannot be used for short packet communication, as these metrics have the underlying assumption of long packet lengths. Ensuring reliable communication and latency requirements for interference-limited scenarios is challenging when devices are constrained to use short packets for communication. In addition to the short size of the packet, data arrival at the users is random in Internet of Things (IoT) or Machine-to-Machine (M2M) communication, which is in contrast to the infinitely backlogged users assumption considered in classical information theory. Thus, capturing the bursty nature of the sources is essential, which can help explore the impact of interference on latency. To address these problems, this work explores the impact of packet length and random data arrival at the transmitter on the system's performance in an interference-limited environment.

This work is licensed under a Creative Commons Attribution 4.0 License. For more information, see https://creativecommons.org/licenses/by/4.0/

There is a need to develop a theory for short-packet communication that considers reliability and latency. Information theory has provided models to capture the uncertainty associated with the underlying channel model, such as noise, fading, and interference. Generally, these works do not capture random data arrival at the users. On the other hand, network theory provides mathematical tools or models to capture the random arrival of data and latency aspects of communication. However, it does not capture the characteristics of the underlying physical channel. Unifying these two theories can provide a more accurate model where it is required to consider the aspects mentioned above jointly [2].

A. RELATED WORKS

To capture the effect of the random arrival of data on the performance, the notion of stable throughput has been used in the existing literature [3], [4], [5], [6]. For multi-user scenarios, stability region becomes a relevant metric. The stability region is analogous to the capacity region in information theory, and it has been explored for many important communication models such as the broadcast channel and interference channel [6], [7]. However, the characterization of stability region in multi-user scenarios is a challenging problem due to interaction among the queues [3], [4]. The technique of stochastic dominance has been used in the existing literature to overcome the difficulty in analyzing interacting queues [3], [6]. The characterization of stability region in systems involving more than two users remains a challenging task.

Latency is another critical aspect for many applications in 5G and beyond communication systems, where the data rate is not the most appropriate key performance index (KPI). Delay and age of Information (AoI) are considered to be relevant metrics to capture latency and timing aspects of information [8]. Delay takes account of transmission and queuing delays in communication. AoI measures the freshness of information [8], [9], [10] and is a relevant metric in status updating systems apparent in IoT and industrial automation scenarios [11].

Characterizing the stability region involves determining the probability of successful decoding at the receiver. In the existing literature, most of the works on stability region either assume that the probability of successful decoding is known or determined using signal to noise ratio (SNR)/ signal to interference plus noise ratio (SINR) based metrics. However, these metrics do not capture the packet length, an essential parameter for reliability and latency requirements in short packet communication. The framework of finite block-length information theory allows to capture the impact of packet length, rate, and power budget at the transmitter and underlying channel model on the error performance [12], [13], [14], [15], [16], [17]. The result in [13] provided the mathematical framework to explore the trade-off between rate, error, and block length for a point-to-point memoryless channel. Progress has also been made in developing the results for multi-user scenarios in the finite block length information theory framework. The second-order achievable rate region for multiple access channels is obtained in [14]. The achievable results for other important models, such as the broadcast and interference channels, can be found in [16], [17]. More details on point-to-point channel and multi-user scenarios under finite block-length regime can be found in [18].

The results from finite-block length information theory have also been used to analyze the performance in case of fading scenario for various communication models [19], [20], [21], [22], [23]. The work in [19] characterizes the average throughput and explores the trade-off between energy efficiency and spectral efficiency for the point-to-point Rayleigh fading channel when no channel state information is available at the transmitter. In general, developing results for multi-user scenarios in the context of short packet communication is a non-trivial problem. In recent years, there has been an increased interest in exploring the role of NOMA in improving the performance metrics such as spectral efficiency in short packet communication [20], [21], [22], [23]. The works in [20], [24] show the benefits of NOMA for downlink scenarios in contrast to the orthogonal counterpart, provided both the schemes use the same block length. The work in [25] proposes opportunistic NOMA for uplink transmission where more than one packet can be sent per slot. The work in [26] explored the throughput of NOMA users in the presence of an external eavesdropper when the users are constrained to use short packets. In [27], stable secure throughput of a Rayleigh faded wiretap channel with a friendly jammer has been characterized for a finite block length coding regime.

When multiple users share a common channel, interference is unavoidable due to the distributed nature of devices. In the existing literature, various interference mitigation techniques, such as treating interference as noise (TIN) and successive interference cancellation (SIC), have been studied extensively for various models under the asymptotic regime [28]. Characterization of second-order coding rates of the Gaussian interference channel (GIC) in the strong interference regime has been considered in [17], and a case where the interference does not affect the channel dispersion has been studied. However, developing a second-order coding rate for the two-user Gaussian IC for general channel conditions still needs to be explored.

B. CONTRIBUTIONS

In short packet communication, various interference mitigation approaches need to take account of the reliability and latency aspects of communication. This paper aims to address the following two related problems:

1) Performance of various interference mitigation techniques, such as TIN, SIC, and joint decoding, are well explored in the existing literature when packets are of large length (for the asymptotic regime). However, the impact of interference on reliability is not well understood when users are constrained to communicate short packets.

2) Performance of various interference mitigation techniques by taking account of random arrival of data at the users, packet length, and underlying physical model is not explored in the existing literature.

To address the above problems, this paper considers a two-user Z-interference channel (Z-IC) under Rayleigh fading, where transmitters can buffer the incoming packets. The metric named stability region is used to capture the bursty nature of the sources. Determination of the stability region requires the characterization of the probability of successful decoding at the receiver. The probabilities of successful decoding for various interference mitigation schemes are characterized for the considered model using the finite block length information theory framework, which allows capturing the impact of packet size and rate on the reliability. The developed results are used to explore the impact of interference on the delay and average age of Information (AAoI) for various interference mitigation techniques. Some works considering delay and stability region under finite block length regime can be found in [29], [30]. The work in [29] explores the benefits of NOMA in reducing queuing delay. It has been shown that SIC may not be an attractive choice for low-latency communication in case of uplink communication under channel uncertainty. The work in [30] examines the stability condition of non-cooperative time-division multiple access (TDMA) and multiple access relay channel with TDMA scheduling and bursty traffic under finite block length constraint. The stability region has been considered for the two-user interference channel in [7]. However, it does not consider the size of the packet in determining the probability of successful decoding. When the arrival of data is random at the users, minimizing only the length of the codeword or packet size in short packet communication may not reduce the delay in communication, as it does not consider the queuing delay. To explore the performance of various interference mitigation schemes in the context of short packet communication, it is required to consider packet size, underlying channel condition, and random arrival rate at the user. The main contributions of the work are summarized below:

1) To capture the bursty arrival of data at the source, the notion of stability region is used, and it is characterized for the considered system model (See Section III). The evaluation of the stability region requires the characterization of the probability of successful decoding at the receiver. To the best of the authors' knowledge, the stability region for the two-user Z-IC has not been explored in the existing literature.
2) The probability of successful decoding at both the receivers corresponding to different queue states is characterized for the two-user Rayleigh fading Z-IC, for various interference mitigation techniques (See Section IV). The results are derived using the finite block-length information theory framework, which captures the packet's length. For the SIC scheme, the derivation of probability of successful decoding takes account of the product of the error terms involved in both the stages of decoding, which is ignored in the existing works to the best of authors' knowledge [23], [29], [31], [32], [33].
3) In addition to the stability region, it is essential to understand how interference affects latency in the case of different interference mitigation schemes. To address this problem, average delay and AAoI are characterized for the considered system model. The developed results help to explore the interplay between average delay and AAoI for various interference mitigation techniques, which needs to be explored in the literature.

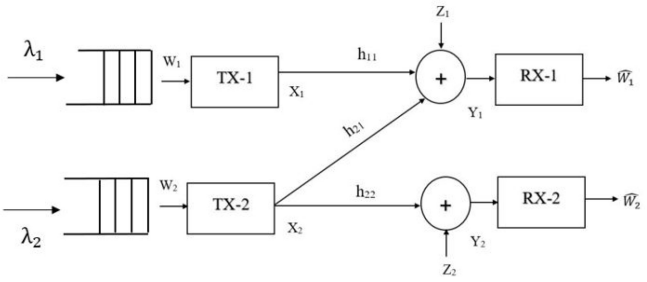

FIGURE 1. Two-user Z-interference channel with queues.

The complete list of notations and mathematical functions used in this work is given in Table 1.

II. SYSTEM MODEL

This work considers a two-user Rayleigh-faded Z-IC with random data arrival at the transmitters, as shown in Fig. 1. Each transmitter has a queue to store the incoming packets. Rx-i is intended to receive packets from Tx-i ($i \in \{1, 2\}$). In Z-IC, only one of the receivers (Rx-1 in this case) experiences interference. Z-IC can be considered as a special case of interference channel, and real-world scenarios can be modeled using Z-IC [34], [35]. Examples of such cases are when one of the users is far from the interfering transmitter or one of the receivers is blocked by an obstacle. In such cases, one of the receivers does not experience interference, whereas the other receiver experiences interference. Time is assumed to be slotted. The packet arrival processes at Tx-1 and Tx-2 are assumed to be stationary and independent with arrival probabilities λ_1 and λ_2 (packets/slot), respectively. Both the transmitters have an infinite capacity to store the incoming packets, and Q_i denotes the length of the queue corresponding to the i^{th} transmitter, $i \in \{1, 2\}$. A transmitter is assumed to send a packet when its queue is non-empty. Otherwise, it remains silent. Packets that arrive at the queue are served on a first come-first serve (FCFS) basis, i.e., FCFS queuing policy is adopted. Even though the last come-first serve (LCFS) queuing policy ensures a relatively lower AoI, it can increase the average delay. This paper aims to give a unified view of the impact of interference on the stability region, average delay, and AoI when users are constrained to use short packets. In applications where the packet arrival

TABLE 1. Notation List.

Notation used	Description
λ_i	Arrival probability at the queue of Tx-i
μ_i	Service probability associated with Tx-i
h_{ij}	Channel coefficient between Tx-i and Rx-j
$G_{ij} \triangleq \lvert h_{ij}\rvert^2$	Square of the magnitude of channel gain between Tx-i and Rx-j
ϕ_{ij}	Average value of channel gain between Tx-i and Rx-j
N	Block length in channel uses
k_i	Number of information nats corresponding to Tx-i
$R_i \triangleq \frac{k_i}{N}$	Rate of Tx-i
P_i	Power corresponding to Tx-i in Watts
$Pr(E)$	Probability of an event E
D_i^{τ}	Event of successfully decoding a packet at Rx-i ($i \in \{1,2\}$) when a packet is sent by Tx-i, given a set of active transmitters denoted by τ
q_i	Random access probability of Tx-i
$V_{NG}(x) \triangleq 1 - \frac{1}{(1+x)^2}$	Dispersion term corresponding to non-Gaussian signaling scheme at the transmitter
$V_G(x) \triangleq \frac{2x}{(1+x)}$	Dispersion term corresponding to Gaussian signaling scheme at the transmitter
SNR	Signal to noise ratio
INR	Interference to noise ratio
SINR	Signal to interference plus noise ratio
Δ_i	Average delay at Rx-i
$AAoI_i$	Average age of Information at Rx-i

order is of prime concern, the FCFS queuing policy is more relevant. Hence, this work adopts an FCFS queuing policy. Further, it is assumed that the acknowledgments (ACKs) are instantaneous and error-free. If a receiver fails to decode its intended packet, it will remain in its queue at the transmitter and be re-transmitted in the next time slot. Re-transmissions at the transmitter are necessary when it is required to receive all the information at the receiver.

Tx-i encodes k_i information nats into a codeword of length N (in channel uses), and the rate is defined as $R_i \triangleq \frac{k_i}{N}$. The power budget at Tx-i is P_i in Watts, ($i \in \{1,2\}$). The channel between the nodes (h_{ij}) are assumed to undergo Rayleigh fading and are independent of each other. Let $\mathbb{1}_{\{A\}}$ denotes indicator variable which takes a value 1 if A is true, otherwise it takes the value 0. Then, the input-output relation for the model is given below:

$$Y_1 = h_{11}X_1\ \mathbb{1}_{\{Q_1>0\}} + h_{21}X_2\ \mathbb{1}_{\{Q_2>0\}} + Z_1, \quad \text{and} \tag{1}$$

$$Y_2 = h_{22}X_2\ \mathbb{1}_{\{Q_2>0\}} + Z_2, \tag{2}$$

where noise Z_i is modelled as a complex additive white Gaussian noise (AWGN), i.e., $Z_i \sim \mathcal{CN}(0,1)$. The system's performance is analyzed in block-fading conditions [36], [37], [38], i.e., where the channel coefficients remain constant during the transmission of the codeword, and then change according to the underlying distribution of the channel. The receivers are assumed to have perfect channel state information (CSI) [37], [38]. However, the transmitter does not know instantaneous channel gain but knows the channel statistics. The probability density function of the square of the magnitude of channel gain ($G_{ij} \triangleq \lvert h_{ij}\rvert^2,\ i,\ j \in \{1,\ 2\}$) follows exponential distribution as given below:

$$f_{G_{ij}}(x) = \frac{1}{\phi_{ij}} e^{-\frac{x}{\phi_{ij}}},\ x \geq 0,\ i,\ j \in \{1,2\}, \tag{3}$$

where ϕ_{ij} represents the average value of channel gain between Tx-i and Rx-j.

III. CHARACTERIZATION OF STABILITY REGION

In many emerging scenarios such as M2M communication or IoT, stability region is a relevant metric as it accounts for random data arrival at the users. *Stability region* is defined as the set of all arrival rates such that all the queues in the system are stable [7]. In the following theorem, the stability region is characterized for the two-user Z-IC without assuming any specific encoding or decoding schemes at the transmitter or receiver, respectively. In this case, Tx-i sends a packet whenever its queue has a packet, i.e., when $Q_i \neq 0$.

In the following theorem, the term D_i^{τ} denotes the event that Rx-i is able to successfully decode the packet sent from Tx-i ($i \in \{1,2\}$) given that a set of transmitters denoted by τ is sending packet. For example, $D_1^{\{1,2\}}$ denotes the event of successfully decoding the packet sent by Tx-1 at Rx-1 provided that both the transmitters ($\tau = \{1,2\}$) are sending packets. Similarly, $D_1^{\{1\}}$ denotes the event of successfully decoding the packet sent by Tx-1 at Rx-1, when only Tx-1 is sending the packets. The term $\mathcal{P}r(D_i^{\tau})$ denotes the probability of event D_i^{τ}. The same notation is used in the rest of the paper.

Theorem 1: The stability region of the two-user Z-IC with bursty arrival of data at the transmitters is given by

$$\mathcal{R} = \Bigg\{(\lambda_1, \lambda_2): \frac{\lambda_1}{\mathcal{P}r\left(D_1^{\{1\}}\right)} + \frac{\left[\mathcal{P}r\left(D_1^{\{1\}}\right) - \mathcal{P}r\left(D_1^{\{1,2\}}\right)\right]\lambda_2}{\mathcal{P}r\left(D_1^{\{1\}}\right)\mathcal{P}r\left(D_2^{\{2\}}\right)} < 1,\ \lambda_2 < \mathcal{P}r\left(D_2^{\{2\}}\right)\Bigg\}. \quad (4)$$

Proof: The service probability μ_i associated with Tx-i ($i \in \{1, 2\}$) is given by the following expression:

$$\mu_1 = \mathcal{P}r(Q_2 > 0)\mathcal{P}r\left(D_1^{\{1,2\}}\right) + \mathcal{P}r(Q_2 = 0)\mathcal{P}r\left(D_1^{\{1\}}\right), \quad (5)$$

$$\mu_2 = \mathcal{P}r\left(D_2^{\{2\}}\right). \quad (6)$$

From (6), one can observe that the service rate corresponding to Rx-2 does not depend on the status of the other queue as there is no interference from Tx-1. Hence, there is no coupling between the queues at the transmitters in the case of Z-IC. From Loyne's criterion [6], it is known that queue at the Tx-2 is stable *if and only if* $\lambda_2 < \mu_2$. Thus, the stability condition for Tx-2 is given by:

$$\lambda_2 < \mu_2, \quad (7)$$

where μ_2 is as given in (6). Note that λ_2 denotes the number of packet arrivals per unit time slot at Tx-2, whereas μ_2 denotes the number of packets that are being serviced at Rx-2 per unit time slot. To determine the service rate corresponding to Rx-1, it is required to determine the probability that queue at Tx-2 is empty ($Pr(Q_2 = 0)$) or non-empty ($Pr(Q_2 > 0)$). From Little's theorem, the probability that queue at Tx-2 is non-empty is given by:

$$Pr(Q_2 > 0) = \frac{\lambda_2}{\mathcal{P}r\left(D_2^{\{2\}}\right)}. \quad (8)$$

Substituting (8) into (5), service rate for Rx-1 is given by:

$$\mu_1 = \mathcal{P}r\left(D_1^{\{1\}}\right) - \frac{\lambda_2\mathcal{P}r\left(D_1^{\{1\}}\right)}{\mathcal{P}r\left(D_2^{\{2\}}\right)} + \frac{\lambda_2\mathcal{P}r\left(D_1^{\{1,2\}}\right)}{\mathcal{P}r\left(D_2^{\{2\}}\right)}. \quad (9)$$

The queue at Tx-1 is stable if and only if $\lambda_1 < \mu_1$, and hence, the stability condition is given by

$$\lambda_1 < \mathcal{P}r\left(D_1^{\{1\}}\right) - \frac{\lambda_2\mathcal{P}r\left(D_1^{\{1\}}\right)}{\mathcal{P}r\left(D_2^{\{2\}}\right)} + \frac{\lambda_2\mathcal{P}r\left(D_1^{\{1,2\}}\right)}{\mathcal{P}r\left(D_2^{\{2\}}\right)}. \quad (10)$$

The stability region $\mathcal{R}$ stated in the theorem is obtained using (10) and (7). ■

Remark: The result mentioned above regarding the stability region holds in general for any interference management technique, and the general form of the stability region is depicted in Fig. 2. Hence, it is necessary to evaluate the probability of successful decoding ($\mathcal{P}r(D_i^{\{\tau\}})$) corresponding to different interference mitigation schemes to determine the stability region. The probability of successful decoding corresponding to different interference mitigation schemes is evaluated in Section IV.

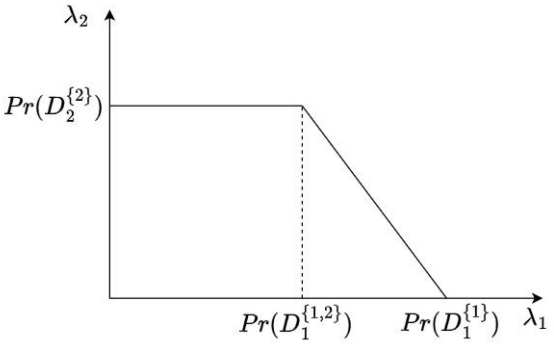

FIGURE 2. Stability region of Z-IC for the general case.

A. STABILITY REGION ANALYSIS WITH RANDOM ACCESS

When users operate in interference-limited scenarios, random access may improve the stability region further. In this case, whenever a transmitter has a packet to send, it sends that packet with a certain probability. Since only one of the transmitters causes interference in the Z-IC, it is assumed that Tx-2 sends a packet using random access protocol, and the other user sends a packet whenever its queue is not empty. The stability region with random access is stated in the following corollary.

Corollary 1: The stability region of the two-user Z-IC with bursty arrival of data at the transmitters and with random access at Tx-2 is given by the following expression:

$$\mathcal{R}^{RA} = \Bigg\{(\lambda_1, \lambda_2): \frac{\lambda_1}{\mathcal{P}r\left(D_1^{\{1\}}\right)} + \frac{\lambda_2\left[\mathcal{P}r\left(D_1^{\{1\}}\right) - \mathcal{P}r\left(D_1^{\{1,2\}}\right)\right]}{\mathcal{P}r\left(D_1^{\{1\}}\right)\mathcal{P}r\left(D_2^{\{2\}}\right)} < 1,\ \lambda_2 < q_2\mathcal{P}r\left(D_2^{\{2\}}\right)\Bigg\}, \quad (11)$$

where Tx-2 sends a packet with probability q_2 ($q_2 \neq 0$), when its queue is non-empty.

Proof: The service probability of user-1 (μ_1) is given by the following expression:

$$\mu_1 = \mathcal{P}r\left(D_1^{\{1,2\}}\right)\mathcal{P}r(\text{Tx-2 is transmitting}) + \mathcal{P}r\left(D_1^{\{1\}}\right)\mathcal{P}r(\text{Tx-2 is not transmitting}). \quad (12)$$

To evaluate μ_1, it is required to determine $\mathcal{P}r$(Tx-2 is transmitting), which is given by:

$$\mathcal{P}r(\text{Tx-2 is transmitting}) = q_2\mathcal{P}r(Q_2 > 0). \quad (13)$$

Hence, the service probability of Tx-1 is simplified to the following:

$$\mu_1 = \mathcal{P}r\left(D_1^{\{1,2\}}\right)q_2\mathcal{P}r(Q_2 > 0) + \mathcal{P}r\left(D_1^{\{1\}}\right)\left[1 - q_2\mathcal{P}r(Q_2 > 0)\right]. \quad (14)$$

It can be seen that service probability of Tx-2 is given by $\mu_2 = q_2\mathcal{P}r(D_2^{\{2\}})$ and from Little's theorem, probability that

queue at Tx-2 is non-empty is given by:

$$\mathcal{P}r(Q_2 > 0) = \frac{\lambda_2}{\mu_2} = \frac{\lambda_2}{q_2 \mathcal{P}r\left(D_2^{\{2\}}\right)}. \tag{15}$$

Substituting (15) in (14), the service probability for user 1 becomes:

$$\frac{\mu_1}{\mathcal{P}r\left(D_1^{\{1\}}\right)} = 1 + \frac{\lambda_2\left[\mathcal{P}r\left(D_1^{\{1,2\}}\right) - \mathcal{P}r\left(D_1^{\{1\}}\right)\right]}{\mathcal{P}r\left(D_1^{\{1\}}\right)\mathcal{P}r\left(D_2^{\{2\}}\right)}. \tag{16}$$

For the queue at Tx-1 to be stable, following condition needs to be satisfied: $\lambda_1 < \mu_1$. Hence, following holds:

$$\frac{\lambda_1}{\mathcal{P}r\left(D_1^{\{1\}}\right)} < \frac{\mu_1}{\mathcal{P}r\left(D_1^{\{1\}}\right)}. \tag{17}$$

Substituting (16) in (17), we obtain:

$$\frac{\lambda_1}{\mathcal{P}r\left(D_1^{\{1\}}\right)} + \frac{\lambda_2\left[\mathcal{P}r\left(D_1^{\{1\}}\right) - \mathcal{P}r\left(D_1^{\{1,2\}}\right)\right]}{\mathcal{P}r\left(D_1^{\{1\}}\right)\mathcal{P}r\left(D_2^{\{2\}}\right)} < 1. \tag{18}$$

Similarly, for the Queue at Tx-2 to be stable, following condition needs to be satisfied:

$$\lambda_2 < q_2 \mathcal{P}r\left(D_2^{\{2\}}\right). \tag{19}$$

Thus, from (18) and (19), stability region of Z-IC with random access at Tx-2 is obtained as stated in the corollary. ■

Remarks:

1) The second inequality in (11) depends on random access probability q_2, whereas the first inequality does not depend on q_2. One can observe that the stability region in (11) is a sub-region of the stability region without random access at Tx-2, i.e., $q_2 = 1$. Hence, random access at Tx-2 does not improve the stability region of the Z-IC.
2) If one seeks to maximize the first user's performance under constraints on the stable throughput of the second user, random access at the second transmitter can still provide benefits, as it regulates the transmission. However, this is out of this work's scope and left as a future extension.
3) When $q_2 = 0$, it can be observed that $\mu_2 = q_2 \mathcal{P}r(D_2^{\{2\}}) = 0$. As Tx-2 does not send any packet irrespective of any new arrival of packets, $\mathcal{P}r(Q_2 > 0) = 1$. Hence, the second queue in the considered system model is unstable for any non-zero arrival rate λ_2. Both the queues in the system need to be stable for the stability region.

IV. PROBABILITY OF SUCCESSFUL DECODING FOR VARIOUS INTERFERENCE MITIGATION TECHNIQUES

In this section, the probability of successful decoding based on the queue states at the transmitters is characterized for the following interference mitigation schemes: (a) *TIN*, (b) *SIC*, and (c) *Joint decoding (JD)*. This, in turn, enables characterizing the stability region of different interference mitigation techniques. In many future applications, such as M2M communication, packet length is short, and it is necessary to consider the packet length in determining the probability of successful decoding. The problem is non-trivial for the following reasons:

1) The probability of successful decoding depends on factors such as rate, packet length, underlying channel model, and interference mitigation techniques at Rx-1. To capture these, this work uses the finite blocklength information theory framework to determine the probability of successful decoding for various interference mitigation schemes.
2) The probability of successful decoding requires the determination of error expression for various decoding schemes, and these results are not explored in the existing literature for the two-user Z-IC under the framework of finite block-length information theory.

This work obtains instantaneous error expression for the corresponding decoding scheme to determine the expression for the average block error rate (BLER). Moreover, the distribution of the signal at the transmitter (or the codeword corresponding to the message) is chosen carefully for mathematical tractability. To the best of the authors' knowledge, the average error for various interference management schemes has yet to be characterized in the literature for the considered model under finite blocklength coding regime.

A. TREATING INTERFERENCE AS NOISE

TIN is one of the conventional schemes to mitigate interference. In addition to its low complexity in decoding, TIN is robust to channel uncertainty. Hence, it is essential to understand the performance of the TIN scheme in different interference regimes under finite block length coding. To characterize the probability of successful decoding at the Rx-1, it is necessary to determine the instantaneous BLER when Rx-1 treats interference as noise. In this case, the channel between Tx-1 and Rx-1 can be modeled as a point-to-point channel with a modified noise variance. The achievable result in [13] uses a non-Gaussian signaling scheme. When both the transmitters use such a non-Gaussian signaling scheme, the effective noise $(h_{21}X_2 + Z_1)$ at Rx-1 is no longer Gaussian, and the model reduces to a non-Gaussian Z-IC, which is hard to analyze. Similar observations have been made regarding multiple access channels in [29]. To overcome this problem, signaling schemes at the transmitters are carefully chosen, and more details in this regard can be found in the proof of the following theorem.

Theorem 2: In a two-user Rayleigh faded Z-IC channel, when Rx-1 treats interference as noise, the probability of successful decoding at the receivers, depending on the status of the queues, are given as follows:

1) When $Q_1 \neq 0$ and $Q_2 \neq 0$:

$$\mathcal{P}r\left(D_1^{\{1,2\}}\right) = 1 - \overline{\epsilon_{TIN}},$$
$$\text{and } \mathcal{P}r\left(D_2^{\{2\}}\right) = 1 - \overline{\epsilon_{22_G}}. \tag{20}$$

2) When $Q_1 \neq 0$ and $Q_2 = 0$:

$$\mathcal{P}r\left(D_1^{\{1\}}\right) = 1 - \overline{\epsilon_{11_{NG}}}. \tag{21}$$

3) When $Q_1 = 0$ and $Q_2 \neq 0$:

$$\mathcal{P}r\left(D_2^{\{2\}}\right) = 1 - \overline{\epsilon_{22_G}}, \tag{22}$$

where

$$\overline{\epsilon_{11_{NG}}} \approx 1 + \beta_{1_{NG}}\phi_{11}P_1\left(e^{-\frac{\left(\alpha_1+\frac{1}{2\beta_{1_{NG}}}\right)}{\phi_{11}P_1}} - e^{-\frac{\left(\alpha_1-\frac{1}{2\beta_{1_{NG}}}\right)}{\phi_{11}P_1}}\right), \tag{23}$$

$$\overline{\epsilon_{TIN}} \approx 1 - \frac{\beta_{1_{NG}}\phi_{11}P_1 e^{\frac{1}{\phi_{21}P_2}}}{\phi_{21}P_2}\left[Ei\left(-\frac{\left(\alpha_1+\frac{1}{2\beta_{1_{NG}}}\right)}{\phi_{11}P_1} - \frac{1}{\phi_{21}P_2}\right) - Ei\left(-\frac{\left(\alpha_1-\frac{1}{2\beta_{1_{NG}}}\right)}{\phi_{11}P_1} - \frac{1}{\phi_{21}P_2}\right)\right], \tag{24}$$

$$\overline{\epsilon_{22_G}} \approx 1 + \beta_{2_G}\phi_{22}P_2\left(e^{-\frac{\left(\alpha_2+\frac{1}{2\beta_{2_G}}\right)}{\phi_{22}P_2}} - e^{-\frac{\left(\alpha_2-\frac{1}{2\beta_{2_G}}\right)}{\phi_{22}P_2}}\right), \tag{25}$$

$$\beta_{1_{NG}} \triangleq \sqrt{\frac{N}{2\pi\left(e^{2R_1}-1\right)}},\ \beta_{2_G} \triangleq \sqrt{\frac{N}{4\pi e^{R_2}\left(e^{R_2}-1\right)}},$$
$$\alpha_i \triangleq e^{R_i} - 1, \text{ and } Ei(x) \triangleq -\int_{-x}^{\infty}\frac{e^{-t}}{t}dt. \tag{26}$$

Proof: The probability of successful decoding based on the status of the queues is evaluated as follows.

a) When $Q_1 \neq 0$ and $Q_2 \neq 0$: In this case, as both the queues have packets to send, Rx-1 is subjected to interference. When Rx-1 treats interference as noise, the noise floor at the receiver increases, and the effective noise is given by $h_{21}X_2 + Z_1$. The achievable result for the point-to-point memoryless channel in [13] uses non-Gaussian signaling. When such signaling is used at both the transmitters, the model reduces to a non-Gaussian Z-IC, as the effective noise $(h_{21}X_2 + Z_1)$ is no longer Gaussian. Analysing non-Gaussian Z-IC is a complex problem. Similar observations have been made in the case of MAC channel [29]. To overcome this problem, Tx-2 uses Gaussian signaling so that the effective noise at Rx-1 $(h_{21}X_2 + Z_1)$ is Gaussian. As the effective noise follows Gaussian distribution, it is possible to use the achievable result in [13] for Rx-1. As non-Gaussian signaling results in smaller dispersion than Gaussian signaling in the finite block-length regime [39], Tx-1 uses non-Gaussian signaling. The probabilities of successful decoding at the receivers are obtained as follows.

Evaluation of $\mathcal{P}r\left(\mathcal{D}_1^{\{1,2\}}\right)$: Let ϵ_{TIN} and $\overline{\epsilon_{TIN}}$ denote the instantaneous BLER and average BLER, respectively in case of TIN scheme at Rx-1. Then

$$\mathcal{P}r\left(D_1^{\{1,2\}}\right) = 1 - \overline{\epsilon_{TIN}}, \tag{27}$$
$$= 1 - E[\epsilon_{TIN}], \tag{28}$$

where ϵ_{TIN} is given by [13]:

$$\epsilon_{TIN} \approx Q\left(\frac{\sqrt{N}\left(\log\left(1+\gamma_{1,TIN}\right) - R_1\right)}{\sqrt{V_{NG}\left(\gamma_{1,TIN}\right)}}\right), \tag{29}$$

$$Q(x) = \frac{1}{\sqrt{2\pi}}\int_x^{\infty} e^{-\frac{t^2}{2}}dt, \tag{30}$$

$$\gamma_{1,TIN} \triangleq \frac{G_{11}P_1}{1+G_{21}P_2}, \text{ and} \tag{31}$$

$$V_{NG}\left(\gamma_{1,TIN}\right) \triangleq 1 - \frac{1}{\left(1+\gamma_{1,TIN}\right)^2}. \tag{32}$$

The term $V_{NG}(\gamma_{1,TIN})$ defined in (32) denotes the channel dispersion term corresponding to the case where Tx-1 transmits non-Gaussian codewords ($\gamma_{1,TIN}$ is the SINR at Rx-1). The subscript NG in $V_{NG}(\gamma_{1,TIN})$ is used to emphasize that Tx-1 uses non-Gaussian signaling. $V(SNR)$ denotes the channel dispersion, which captures the variability of the channel relative to a deterministic bit pipe with the same capacity. Channel dispersion is a function of SNR and varies according to the signaling scheme employed at the transmitter. Note that in (29) higher order terms $O(\frac{\log n}{n})$ has been ignored. For more details, one can refer to [13], [19], [30]. In the subsequent analysis, such higher order terms are not considered.

To evaluate the average BLER, it is required to calculate the average of the instantaneous BLER with respect to the distribution of the SINR ($\Gamma_{1,TIN}$). As Q-function is involved in (29), it is difficult to find a closed form expression for $\overline{\epsilon_{TIN}}$. By using the linear approximation of Q-function, $\overline{\epsilon_{TIN}}$ can be approximated with (24) as given in the statement of Theorem 2. The details of the linearization approximation of the Q-function and the derivation of average BLER ($\overline{\epsilon_{TIN}}$) can be found in Appendix A. In the following, the probability of successful decoding at Rx-2 is derived.

Evaluation of $\mathcal{P}r(\mathcal{D}_2^{\{2\}})$: Let ϵ_{22_G} denotes the instantaneous BLER at Rx-2 and is given by the following equation [39]:

$$\epsilon_{22_G} \approx Q\left(\frac{\sqrt{N}(\log(1+\gamma_{22}) - R_2)}{\sqrt{V_G(\gamma_{22})}}\right), \tag{33}$$

$$\text{where } \gamma_{22} = G_{22}P_2, \text{ and } V_G(\gamma_{22}) = \frac{2\gamma_{22}}{(1+\gamma_{22})}. \tag{34}$$

The term $V_G(\gamma_{22})$ defined in (34) denotes the channel dispersion term corresponding to the case where Tx-2 sends Gaussian codewords. The subscript G in $V_G(\gamma_{22})$ is used to emphasize that Tx-2 uses Gaussian signaling. One can notice that ϵ_{22_G} does not depend on status of the queue at Tx-1 as there is no interference at Rx-2. Hence,

$$\mathcal{P}r\left(D_2^{\{2\}}\right) = 1 - \overline{\epsilon_{22_G}}, \tag{35}$$
$$= 1 - E\left[\epsilon_{22_G}\right]. \tag{36}$$

Note that the dispersion term $V_G(x)$ in (34) is different from the dispersion term $V_{NG}(x)$ in (32), as Tx-2 uses Gaussian signaling. Hence, the following is used as linear approximation for the Q-function in (33) instead of (104):

$$Q\left(\frac{\sqrt{N}(\log(1+x)-R)}{\sqrt{V_G(x)}}\right) \simeq U_G(x),$$

where

$$U_G(x) \triangleq \begin{cases} 1, & x \leq \alpha - \frac{1}{2\beta_G}, \\ \rho_G - \beta_G x, & x \in \left[\alpha - \frac{1}{2\beta_G}, \alpha + \frac{1}{2\beta_G}\right], \\ 0, & x \geq \alpha + \frac{1}{2\beta_G}. \end{cases} \tag{37}$$

$$\alpha \triangleq e^R - 1, \ \rho_G \triangleq \frac{1}{2} + \alpha\beta_G, \text{ and}$$

$$\beta_G \triangleq -\left.\frac{\partial\left(Q\left(\frac{\sqrt{N}(\log(1+x)-R)}{\sqrt{\frac{2x}{(1+x)}}}\right)\right)}{\partial x}\right|_{x=\alpha} = \sqrt{\frac{N}{4\pi e^R(e^R-1)}}. \tag{38}$$

To determine the average BLER at Rx-2, it is required to determine the cumulative distribution function associated with the SNR (Γ_{22}) at Rx-2, and it is given by

$$\begin{aligned} F_{\Gamma_{22}}(x) &= \mathcal{P}r(G_{22}P_2 \leq x), \\ &= \left(1 - e^{-\frac{x}{\phi_{22}P_2}}\right), \quad x \geq 0. \end{aligned} \tag{39}$$

It can be seen that $F_{\Gamma_{22}}(x)$ can be obtained from $F_{\Gamma_{1,TIN}}(x)$ by substituting $P_2 = 0$ and by replacing P_1 and ϕ_{11} with P_2 and ϕ_{22}, respectively in (105). Hence, the average BLER at Rx-2 ($\overline{\epsilon_{22_G}}$) can be obtained from (107) by substituting $P_2 = 0$ and by replacing α_1, $\beta_{1_{NG}}$, ϕ_{11}, and P_1 with α_2, β_{2_G}, ϕ_{22}, and P_2, respectively and after some simplification, the expression in (25) is obtained.

b) When $Q_1 \neq 0$ and $Q_2 = 0$: As queue 2 is empty, Rx-1 does not experience any interference due to Tx-2. It is required to determine the probability of successful decoding for Rx-1 only. It is obtained as follows:

$$\begin{aligned} \mathcal{P}r\left(D_1^{\{1\}}\right) &= 1 - \overline{\epsilon_{11_{NG}}}, \\ &= 1 - E\left[\epsilon_{11_{NG}}\right], \end{aligned} \tag{40}$$

where $\epsilon_{11_{NG}}$ denotes the instantaneous BLER at Rx-1 when only Tx-1 is active and is given by the following equation [13]:

$$\epsilon_{11_{NG}} \approx Q\left(\frac{\sqrt{N}(\log(1+\gamma_{11})-R_1)}{\sqrt{V_{NG}(\gamma_{11})}}\right), \tag{41}$$

$$\text{where} \quad \gamma_{11} = G_{11}P_1 \text{ and } V_{NG}(\gamma_{11}) = 1 - \frac{1}{(1+\gamma_{11})^2}. \tag{42}$$

By observing the expressions of ϵ_{22_G} and $\epsilon_{11_{NG}}$ stated in (33) and (41) respectively, it can be seen that $\overline{\epsilon_{11_{NG}}}$ stated in (23) can be obtained from the expression of $\overline{\epsilon_{22_G}}$ by replacing P_2, ϕ_{22}, α_2, and β_{2_G} in (25) with P_1, ϕ_{11}, α_1, and $\beta_{1_{NG}}$ respectively.

c) When $Q_1 = 0$ and $Q_2 \neq 0$: In this case, Rx-1 does not receive any packet from Tx-1. It is required to determine the probability of successful decoding only in the case of Rx-2. One can notice that $\mathcal{P}r(D_2^{\{2\}})$ is the same as in the first case, i.e., (36) (where both the transmitters have packets to send). ■

B. SUCCESSIVE INTERFERENCE CANCELLATION SCHEME

In successive interference cancellation, decoding occurs in two stages. In the first stage, Rx-1 decodes the codeword of Tx-2 and treats its intended message as noise. In the second stage, Rx-1 decodes its message after subtracting the interference caused due to Tx-2. As the decoding happens in two stages, the average error must consider the error in both stages. In this work, the expression for the probability of successful decoding for SIC scheme is obtained by taking account of coupling between the errors in both stages, which has been ignored in earlier works [23], [29], [31], [32], [33]. This provides accurate error expression for SIC, as discussed in the later part of the paper.

Theorem 3: In a two-user Rayleigh faded Z-IC channel, when Rx-1 employs the SIC scheme, the probability of successful decoding at the receivers, depending on the status of queues, are given as follows:

1) When $Q_1 \neq 0$ and $Q_2 \neq 0$:

$$\begin{aligned} \mathcal{P}r\left(D_1^{\{1,2\}}\right) &= 1 - \overline{\epsilon_{SIC}}, \\ \text{and } \mathcal{P}r\left(D_2^{\{2\}}\right) &= 1 - \overline{\epsilon_{22_G}}. \end{aligned} \tag{43}$$

2) When $Q_1 \neq 0$ and $Q_2 = 0$:

$$\mathcal{P}r\left(D_1^{\{1\}}\right) = 1 - \overline{\epsilon_{11_G}}. \tag{44}$$

3) When $Q_1 = 0$ and $Q_2 \neq 0$:

$$\mathcal{P}r\left(D_2^{\{2\}}\right) = 1 - \overline{\epsilon_{22_G}}, \tag{45}$$

where different error probabilities are defined at the bottom of next page.

Proof: The probabilities of successful decoding based on the status of the queues are evaluated as follows:

a) When $Q_1 \neq 0$ and $Q_2 \neq 0$: When both the queues are active, Tx-2 creates interference at Rx-1. In this case, both the transmitters send the codewords drawn from Gaussian distribution, and this also ensures that Tx-2 does not cause non-Gaussian interference at Rx-1. The probabilities of successful decoding at both receivers are obtained as follows.

Evaluation of $\mathcal{P}r(D_1^{\{1,2\}})$: In this case, probability of successful decoding at Rx-1 is given by:

$$\begin{aligned} \mathcal{P}r\left(D_1^{\{1,2\}}\right) &= 1 - \overline{\epsilon_{SIC}}, & (52) \\ &= 1 - E[\epsilon_{SIC}], & (53) \end{aligned}$$

where ϵ_{SIC} denotes instantaneous BLER associated with the SIC scheme at Rx-1.

Let E_1 represents the error event in decoding the codeword of Tx-2 at Rx-1, while the codeword of Tx-1 is treated as noise, and E_2 represents error event in decoding codeword of

Tx-1 at Rx-1, then the instantaneous BLER ϵ_{SIC} is obtained as follows:

$$\begin{aligned}\epsilon_{SIC} &= \mathcal{P}r(E_2),\\ &= \mathcal{P}r(E_2|E_1)\mathcal{P}r(E_1) + \mathcal{P}r\left(E_2|E_1^C\right)\mathcal{P}r\left(E_1^C\right),\\ &\simeq 1.\epsilon_{21} + \epsilon_{11_G}(1-\epsilon_{21}),\\ &= \epsilon_{21} + \epsilon_{11_G} - \epsilon_{21}\epsilon_{11_G}. \end{aligned} \tag{54}$$

Here, ϵ_{21} denotes the instantaneous BLER in the first stage of decoding, i.e., while decoding codeword of Tx-2 at Rx-1, and ϵ_{11_G} denotes the instantaneous BLER in decoding the codeword of Tx-1 at Rx-1 (second stage of decoding). When there is an error in the first stage of decoding in SIC, there will be an error in the second stage with high probability, and hence, $\mathcal{P}r(E_2|E_1)$ is set to 1 in the above equation. The term $\epsilon_{21}\epsilon_{11_G}$ was ignored in [29] while evaluating the average error, and this term is taken into account for the calculation of the average BLER in this work.

In the first stage of SIC, the codeword of Tx-2 is decoded by treating the codeword from Tx-1 as noise. In this case, both the transmitters use Gaussian signaling. In the first stage of SIC decoding, the effective noise is given by $h_{11}X_1 + Z_1$. For a given channel realization, h_{ij} are modeled as constant, and hence, $h_{11}X_1 + Z_1$ is modeled as Gaussian noise. Hence, the channel between Tx-2 and Rx-1 can be modeled as an AWGN channel with an equivalent SINR γ_{21} which is defined in (56), for a given realization of h_{11} and h_{21}. Hence, the instantaneous BLER in decoding the codeword of Tx-2 in the first stage can be obtained by replacing γ_{22} in (33) by γ_{21} and the corresponding instantaneous BLER is given by the following expression [39]:

$$\epsilon_{21} \approx Q\left(\frac{\sqrt{N}(\log(1+\gamma_{21}) - R_2)}{\sqrt{\frac{2\gamma_{21}}{1+\gamma_{21}}}}\right) \approx U_G(\gamma_{21}), \tag{55}$$

where $U_G(\gamma_{21})$ is as defined in (37), and

$$\gamma_{21} \triangleq \frac{G_{21}P_2}{1+G_{11}P_1}. \tag{56}$$

Note that SINR γ_{21} in (56) and SINR $\gamma_{1,TIN}$ in (31) are of same form except that G_{11}, G_{21}, P_1, and P_2 are replaced by G_{21}, G_{11}, P_2, and P_1, respectively. Hence, the average BLER $\overline{\epsilon_{21}}$ stated in (46), shown at the bottom of the page can be obtained in the same way as $\overline{\epsilon_{TIN}}$ that was found in TIN scheme by replacing α_1 and $\beta_{1_{NG}}$ with α_2 and β_{2_G}, respectively and the terms P_1 (and ϕ_{11}) need to be interchanged with P_2 (and ϕ_{21}) in (24).

$$\overline{\epsilon_{SIC}} = \overline{\epsilon_{21}} + \overline{\epsilon_{11_G}} - \overline{\epsilon_{21}\epsilon_{11_G}},$$

$$\overline{\epsilon_{21}} \approx 1 - \frac{\beta_{2_G}\phi_{21}P_2 e^{\frac{1}{\phi_{11}P_1}}}{\phi_{11}P_1}\left(\mathrm{Ei}\left(\frac{-\delta_2^u}{\phi_{21}P_2} - \frac{1}{\phi_{11}P_1}\right) - \mathrm{Ei}\left(\frac{-\delta_2^l}{\phi_{21}P_2} - \frac{1}{\phi_{11}P_1}\right)\right), \tag{46}$$

$$\overline{\epsilon_{11_G}} \approx 1 + \beta_{1_G}\phi_{11}P_1\left(e^{-\frac{\left(\alpha_1 + \frac{1}{2\beta_{1_G}}\right)}{\phi_{11}P_1}} - e^{-\frac{\left(\alpha_1 - \frac{1}{2\beta_{1_G}}\right)}{\phi_{11}P_1}}\right), \tag{47}$$

$$\begin{aligned}\overline{\epsilon_{21}\epsilon_{11_G}} \approx{}& \left(1 - e^{-\frac{\delta_1^l}{\phi_{11}P_1}}\right) + \frac{\beta_{2_G}\phi_{21}P_2 e^{\frac{1}{\phi_{11}P_1}}}{\phi_{11}P_1}\left[Ei\left(-\left(1+\delta_1^l\right)h\left(\delta_2^u\right)\right) - Ei\left(-h\left(\delta_2^u\right)\right) - Ei\left(-\left(1+\delta_1^l\right)h\left(\delta_2^l\right)\right)\right.\\ &\left. + Ei\left(-h\left(\delta_2^l\right)\right)\right] + \rho_{1_G}\left(e^{-\frac{\delta_1^l}{\phi_{11}P_1}} - e^{-\frac{\delta_1^u}{\phi_{11}P_1}}\right) + \frac{\rho_{1_G}\beta_{2_G}\phi_{21}P_2 e^{\frac{1}{\phi_{11}P_1}}}{\phi_{11}P_1}\left[Ei\left(-\left(1+\delta_1^u\right)h\left(\delta_2^u\right)\right)\right.\\ &\left. - Ei\left(-\left(1+\delta_1^l\right)h\left(\delta_2^u\right)\right) - Ei\left(-\left(1+\delta_1^u\right)h\left(\delta_2^l\right)\right) + Ei\left(-\left(1+\delta_1^l\right)h\left(\delta_2^l\right)\right)\right] - \beta_{1_G}\left(\delta_1^l + \phi_{11}P_1\right)e^{-\frac{\delta_1^l}{\phi_{11}P_1}}\\ &+ \beta_{1_G}\left(\delta_1^u + \phi_{11}P_1\right)e^{-\frac{\delta_1^u}{\phi_{11}P_1}} - \frac{\beta_{1_G}\beta_{2_G}\phi_{21}P_2 e^{\frac{-\delta_2^u}{\phi_{21}P_2}}}{\phi_{11}P_1}\left[e^{h\left(\delta_2^u\right)}\left(Ei\left(-\left(1+\delta_1^l\right)h\left(\delta_2^u\right)\right) - Ei\left(-\left(1+\delta_1^u\right)h\left(\delta_2^u\right)\right)\right)\right.\\ &\left. - \frac{e^{-\delta_1^u h\left(\delta_2^u\right)}}{h\left(\delta_2^u\right)} + \frac{e^{-\delta_1^l h\left(\delta_2^u\right)}}{h\left(\delta_2^u\right)}\right] + \frac{\beta_{1_G}\beta_{2_G}\phi_{21}P_2 e^{\frac{-\delta_2^l}{\phi_{21}P_2}}}{\phi_{11}P_1}\left[e^{h\left(\delta_2^l\right)}\left(Ei\left(-\left(1+\delta_1^l\right)h\left(\delta_2^l\right)\right) - Ei\left(-\left(1+\delta_1^u\right)h\left(\delta_2^l\right)\right)\right)\right.\\ &\left. - \frac{e^{-\delta_1^u h\left(\delta_2^l\right)}}{h\left(\delta_2^l\right)} + \frac{e^{-\delta_1^l h\left(\delta_2^l\right)}}{h\left(\delta_2^l\right)}\right], \end{aligned} \tag{48}$$

$$\overline{\epsilon_{22_G}} \approx 1 + \beta_{2_G}\phi_{22}P_2\left(e^{-\frac{\left(\alpha_2 + \frac{1}{2\beta_{2_G}}\right)}{\phi_{22}P_2}} - e^{-\frac{\left(\alpha_2 - \frac{1}{2\beta_{2_G}}\right)}{\phi_{22}P_2}}\right), \tag{49}$$

$$\delta_i^l \triangleq \alpha_i - \frac{1}{2\beta_{i_G}},\ \delta_i^u \triangleq \alpha_i + \frac{1}{2\beta_{i_G}},\ \rho_{i_G} \triangleq \frac{1}{2} + \alpha_i\beta_{i_G},\ i \in \{1,2\}, \tag{50}$$

$$h\left(\delta_2^l\right) \triangleq \frac{1}{\phi_{11}P_1} + \frac{\delta_2^l}{\phi_{21}P_2},\ \text{and}\ h\left(\delta_2^u\right) \triangleq \frac{1}{\phi_{11}P_1} + \frac{\delta_2^u}{\phi_{21}P_2}. \tag{51}$$

Instantaneous BLER in the second stage of decoding, i.e., ϵ_{11_G} is given by

$$\epsilon_{11_G} \approx Q\left(\frac{\sqrt{N}(\log(1+\gamma_{11})-R_1)}{\sqrt{\frac{2\gamma_{11}}{1+\gamma_{11}}}}\right) \approx U_G(\gamma_{11}). \quad (57)$$

where $U_G(\gamma_{11})$ is as defined in (37), and

$$\gamma_{11} \triangleq G_{11}P_1. \quad (58)$$

Noticing the similarity between γ_{11} in (58) and γ_{22} in (34), the average BLER $\overline{\epsilon_{11_G}}$ defined in (47), shown at the bottom of the previous page is evaluated in the same way as that of average BLER $\overline{\epsilon_{22_G}}$ and is obtained by replacing α_2, ϕ_{22}, P_2, and β_{2_G} with α_1, ϕ_{11}, P_1, and β_{1_G}, respectively in (25).

Now, consider the evaluation of $E[\epsilon_{21}\epsilon_{11_G}]$:

$$\overline{\epsilon_{21}\epsilon_{11_G}} = E\left[\epsilon_{21}\epsilon_{11_G}\right], = \int_0^\infty \int_0^\infty \epsilon_{21}\epsilon_{11_G} f_{\Gamma_{21},\Gamma_{11}}(\gamma_{21},\gamma_{11})\, d\gamma_{21}\, d\gamma_{11}. \quad (59)$$

To determine $\overline{\epsilon_{21}\epsilon_{11_G}}$, knowledge of the joint density function of Γ_{21} and Γ_{11} ($f_{\Gamma_{21},\Gamma_{11}}(\gamma_{21},\gamma_{11})$) is required and it is obtained as follows:

$$f_{\Gamma_{21},\Gamma_{11}}(\gamma_{21},\gamma_{11}) = f_{\Gamma_{21}|\Gamma_{11}}(\gamma_{21}|\gamma_{11}) f_{\Gamma_{11}}(\gamma_{11}), \quad (60)$$

where

$$f_{\Gamma_{21}|\Gamma_{11}}(\gamma_{21}|\gamma_{11}) = \left(\frac{1+\gamma_{11}}{P_2\phi_{21}}\right) e^{-\frac{1}{\phi_{21}}\left(\frac{\gamma_{21}(1+\gamma_{11})}{P_2}\right)}, \quad (61)$$

and

$$f_{\Gamma_{11}}(\gamma_{11}) = \frac{1}{\phi_{11}P_1} e^{-\frac{\gamma_{11}}{\phi_{11}P_1}}. \quad (62)$$

Using (61) and (62), (60) simplifies to the following:

$$f_{\Gamma_{21},\Gamma_{11}}(\gamma_{21},\gamma_{11}) = \left(\frac{1+\gamma_{11}}{\phi_{21}\phi_{11}P_1P_2}\right) e^{-\frac{\gamma_{21}(1+\gamma_{11})}{\phi_{21}P_2}} e^{-\frac{\gamma_{11}}{\phi_{11}P_1}}. \quad (63)$$

With a slight abuse of notation, the probability density function $f_X(x)$ is presented as $f(x)$ in the rest of the derivation of the theorem. Similarly, $f_{X|Y}(x|y)$ is represented as $f(x|y)$. Using (63), the term $\overline{\epsilon_{21}\epsilon_{11_G}}$ in (59) is approximated with the expression given in (48), shown at the bottom of the previous page. The details of the derivation can be found in Appendix B. In the following, the probability of successful decoding at Rx-2 is derived.

Evaluation of $\mathcal{P}r(\mathcal{D}_2^{\{2\}})$: Probability of successful decoding at Rx-2 is given by

$$\mathcal{P}r\left(D_2^{\{2\}}\right) = 1 - \overline{\epsilon_{22_G}}, \quad (64)$$

$$= 1 - E\left[\epsilon_{22_G}\right], \quad (65)$$

where ϵ_{22_G} is the instantaneous BLER in decoding the codeword of Tx-2 at Rx-2 as defined in (34). Hence, it is evident that $\overline{\epsilon_{22_G}}$ defined in (49), shown at the bottom of the previous page is same as that defined in (25).

b) When $Q_1 \neq 0$ and $Q_2 = 0$: In this case, Tx-2 does not cause any interference to Rx-1. The probability of successful decoding at Rx-1 in this scenario is given by

$$\mathcal{P}r\left(D_1^{\{1\}}\right) = 1 - \overline{\epsilon_{11_G}}, \quad (66)$$

$$= 1 - E\left[\epsilon_{11_G}\right], \quad (67)$$

where ϵ_{11_G} is the instantaneous BLER in decoding the codeword of Tx-1 at Rx-1 as in (57). Note that $\overline{\epsilon_{11_G}}$ corresponds to (47).

c) When $Q_1 = 0$ and $Q_2 \neq 0$: In this case, queue 1 is empty and it is required to consider decoding only at Rx-2. The probability of successful decoding at Rx-2 is given by

$$\mathcal{P}r\left(D_2^{\{2\}}\right) = 1 - \overline{\epsilon_{22_G}}, \quad (68)$$

where $\overline{\epsilon_{22_G}}$ is same as (25), which is characterized when both the queues are active. ■

C. JOINT DECODING SCHEME

Joint decoding scheme requires decoding all the messages simultaneously. In the joint decoding scheme, Rx-1 needs to decode messages of Tx-1 and Tx-2 simultaneously. The joint decoding scheme needs to consider all codeword pairs for optimal decoding. To reduce joint-decoding complexity, one can consider iterative decoding [40], [41]. An example of joint decoding can be found in [40]. The channel between Tx-1, Tx-2, and Rx-1 is modeled as a multiple access channel (MAC), and the result derived in [14] is used to characterize the average error for the joint decoding scheme. To the best of the authors' knowledge, the performance of the joint-decoding scheme under finite block length coding for the Z-interference channel is yet to be explored in the existing literature. The probabilities of successful decoding at both the receivers, corresponding to the joint decoding scheme are stated in the following theorem.

Theorem 4: In the two-user Rayleigh faded Z-IC, when Rx-1 uses a joint decoding scheme, the different probabilities of successful decoding at the receivers depending on the status of queues are given as follows:

1) When $Q_1 \neq 0$ and $Q_2 \neq 0$:

$$\mathcal{P}r\left(D_1^{\{1,2\}}\right) = 1 - \overline{\epsilon_J},$$
$$\text{and } \mathcal{P}r\left(D_2^{\{2\}}\right) = 1 - \overline{\epsilon_{22_{NG}}}. \quad (69)$$

2) When $Q_1 \neq 0$ and $Q_2 = 0$:

$$\mathcal{P}r\left(D_1^{\{1\}}\right) = 1 - \overline{\epsilon_I}. \quad (70)$$

3) When $Q_1 = 0$ and $Q_2 \neq 0$:

$$\mathcal{P}r\left(D_2^{\{2\}}\right) = 1 - \overline{\epsilon_{22_{NG}}}, \quad (71)$$

where

$$\overline{\epsilon_J} = \overline{\epsilon_I} + \overline{\epsilon_{II}} + \overline{\epsilon_{III}}, \quad (72)$$

$$\overline{\epsilon_I} \triangleq 1 + \beta_{1_{NG}}\phi_{11}P_1\left(e^{-\frac{\alpha_1+\frac{1}{2\beta_{1_{NG}}}}{\phi_{11}P_1}} - e^{-\frac{\alpha_1-\frac{1}{2\beta_{1_{NG}}}}{\phi_{11}P_1}}\right), \quad (73)$$

$$\overline{\epsilon_{II}} \triangleq 1 + \beta_{2_{NG}}\phi_{21}P_2\left(e^{-\frac{\alpha_2+\frac{1}{2\beta_{2_{NG}}}}{\phi_{21}P_2}} - e^{-\frac{\alpha_2-\frac{1}{2\beta_{2_{NG}}}}{\phi_{21}P_2}}\right), \quad (74)$$

$$\overline{\epsilon_{III}} \triangleq 1-\frac{(\phi_{11}P_1)^2\beta_{3_{NG}}}{(\phi_{11}P_1-\phi_{21}P_2)}\left(e^{-\frac{\left(\alpha_3-\frac{1}{2\beta_{3_{NG}}}\right)}{\phi_{11}P_1}}-e^{-\frac{\left(\alpha_3+\frac{1}{2\beta_{3_{NG}}}\right)}{\phi_{11}P_1}}\right)+\frac{(\phi_{21}P_2)^2\beta_{3_{NG}}}{(\phi_{11}P_1-\phi_{21}P_2)}\left(e^{-\frac{\left(\alpha_3-\frac{1}{2\beta_{3_{NG}}}\right)}{\phi_{21}P_2}}-e^{-\frac{\left(\alpha_3+\frac{1}{2\beta_{3_{NG}}}\right)}{\phi_{21}P_2}}\right), \tag{75}$$

$$\overline{\epsilon_{22_{NG}}} \triangleq 1+\beta_{2_{NG}}\phi_{22}P_2\left(e^{-\frac{\alpha_2+\frac{1}{2\beta_{2_{NG}}}}{\phi_{22}P_2}}-e^{-\frac{\alpha_2-\frac{1}{2\beta_{2_{NG}}}}{\phi_{22}P_2}}\right), \tag{76}$$

$$\alpha_i \triangleq e^{R_i}-1,\ \ i\in\{1,2\},\ \ \beta_{1_{NG}} \triangleq \sqrt{\frac{N}{2\pi\left(e^{2R_1}-1\right)}},$$
$$\beta_{2_{NG}} \triangleq \sqrt{\frac{N}{2\pi\left(e^{2R_2}-1\right)}},\ \ \alpha_3 \triangleq e^{(R_1+R_2)}-1,$$
$$\text{and } \beta_{3_{NG}} \triangleq \sqrt{\frac{N}{2\pi\left(e^{2(R_1+R_2)}-1\right)}}. \tag{77}$$

Proof: The different probabilities of successful decoding are evaluated in the following cases:

a) When $Q_1 \neq 0$ and $Q_2 \neq 0$: When both the transmitters have a packet to send, one can see that Tx-1, Tx-2, and Rx-1 form a MAC channel. Rx-1 can use the joint decoding scheme to decode its message. Using the result for the MAC channel [14], [42], the rates R_1 and R_2 are achievable with instantaneous BLER $\epsilon_J = \epsilon_I + \epsilon_{II} + \epsilon_{III}$ and the following holds:

$$\epsilon_I \leq Q\left(\frac{\sqrt{N}\left(\log\left(1+\gamma_{1_J}\right)-R_1\right)}{\sqrt{V_{NG}\left(\gamma_{1_J}\right)}}\right),$$
$$\epsilon_{II} \leq Q\left(\frac{\sqrt{N}\left(\log\left(1+\gamma_{2_J}\right)-R_2\right)}{\sqrt{V_{NG}\left(\gamma_{2_J}\right)}}\right),$$
$$\epsilon_{III} \leq Q\left(\frac{\sqrt{N}\left(\log\left(1+\gamma_{t_J}\right)-(R_1+R_2)\right)}{\sqrt{V\left(\gamma_{1_J},\gamma_{2_J}\right)}}\right), \tag{78}$$

where

$$\gamma_{1_J} = |h_{11}|^2P_1, \tag{79}$$
$$\gamma_{2_J} = |h_{21}|^2P_2, \tag{80}$$
$$\gamma_{t_J} = \gamma_{1_J}+\gamma_{2_J}, \tag{81}$$
$$V_{NG}\left(\gamma_{i_J}\right) = 1-\frac{1}{\left(1+\gamma_{i_J}\right)^2},\ \ i\in\{1,2\}, \tag{82}$$
$$\text{and } V\left(\gamma_{1_J},\ \gamma_{2_J}\right) = V_{NG}\left(\gamma_{1_J}+\gamma_{2_J}\right)+\frac{2\gamma_{1_J}\gamma_{2_J}}{\left(1+\gamma_{1_J}+\gamma_{2_J}\right)^2}. \tag{83}$$

As it is difficult to evaluate the error probability ϵ_I, ϵ_{II}, and ϵ_{III} exactly, each error term is set equal to the RHS in (78). The probability of successful decoding is given by

$$\mathcal{P}r\left(D_1^{\{1,2\}}\right) = 1-\overline{\epsilon_J}, \tag{84}$$

where

$$\overline{\epsilon_J} = E[\epsilon_J],$$
$$= \underbrace{E[\epsilon_I]}_{\triangleq\overline{\epsilon_I}}+\underbrace{E[\epsilon_{II}]}_{\triangleq\overline{\epsilon_{II}}}+\underbrace{E[\epsilon_{III}]}_{\triangleq\overline{\epsilon_{III}}}. \tag{85}$$

Since each error term is set equal to RHS in (78), $\overline{\epsilon_J}$ in (85) can be greater than the actual error probability. Thus, the probability of successful decoding obtained using $\overline{\epsilon_J}$ is a lower bound. A minimum of average error probability and 1 is considered for the numerical evaluation and simulation.

First consider the evaluation for $\overline{\epsilon_I}$. By noticing the similarity between the expressions of ϵ_I stated in (78) and $\epsilon_{11_{NG}}$ stated in (41), it can be seen that $\overline{\epsilon_I}$ defined in (73) can be obtained by following similar approach as used for deriving $\overline{\epsilon_{11_{NG}}}$ in Theorem 2. By noticing the similarity between the expressions of ϵ_{II} stated in (78) and $\epsilon_{11_{NG}}$ stated in (41), it can be seen that $\overline{\epsilon_{II}}$ defined in (74) can be obtained by following similar approach as used for deriving $\overline{\epsilon_{11_{NG}}}$ in Theorem 2.

Determining the average BLER $\overline{\epsilon_{III}}$) is non-trivial due to the involvement of the Q-function and the term $V(\gamma_{1_J},\gamma_{2_J})$ is defined as follows:

$$V\left(\gamma_{1_J},\gamma_{2_J}\right) = V_{NG}\left(\gamma_{1_J}+\gamma_{2_J}\right)+\frac{2\gamma_{1_J}\gamma_{2_J}}{\left(1+\gamma_{1_J}+\gamma_{2_J}\right)^2}, \tag{86}$$
$$\simeq V_{NG}\left(\gamma_{1_J}+\gamma_{2_J}\right). \tag{87}$$

The term $V_{NG}(\gamma_{1_J}+\gamma_{2_J})$ can also be expressed in the following manner:

$$V_{NG}\left(\gamma_{1_J}+\gamma_{2_J}\right) = 1-\frac{1}{\left(1+\gamma_{1_J}+\gamma_{2_J}\right)^2}, \tag{88}$$
$$= \frac{\gamma_{1_J}^2+\gamma_{2_J}^2+2\gamma_{1_J}+2\gamma_{2_J}}{\left(1+\gamma_{1_J}+\gamma_{2_J}\right)^2}+\frac{2\gamma_{1_J}\gamma_{2_J}}{\left(1+\gamma_{1_J}+\gamma_{2_J}\right)^2}. \tag{89}$$

From the above equation, it can be seen that the approximation in (87) is accurate when the following condition is satisfied:

$$\frac{\gamma_{1_J}^2+\gamma_{2_J}^2+2\gamma_{1_J}+2\gamma_{2_J}}{\left(1+\gamma_{1_J}+\gamma_{2_J}\right)^2}+\frac{2\gamma_{1_J}\gamma_{2_J}}{\left(1+\gamma_{1_J}+\gamma_{2_J}\right)^2} >> \frac{2\gamma_{1_J}\gamma_{2_J}}{\left(1+\gamma_{1_J}+\gamma_{2_J}\right)^2},$$
$$\text{or}\quad \gamma_{1_J}^2+\gamma_{2_J}^2+2\gamma_{1_J}+2\gamma_{2_J} >> 0. \tag{90}$$

The above condition is satisfied when at least one of the terms γ_{1_J} or γ_{2_J} is large. The second term of $V_{NG}(\gamma_{1_J},\gamma_{2_J})$, i.e., $\frac{2\gamma_{1_J}\gamma_{2_J}}{(1+\gamma_{1_J}+\gamma_{2_J})^2}$ is a ratio of the product of SNR (γ_{1_J}) and INR (γ_{2_J}), and square of the sum of SNR and INR. Due to this, obtaining a closed-form expression for $\overline{\epsilon_{III}}$ becomes difficult. Hence, the second term in (86) is ignored in the evaluation of $E[\epsilon_{III}]$ for mathematical tractability. However, this term has been considered in the simulation, and a close

match has been found between the simulation and numerical results (See Section VI).

To determine $\overline{\epsilon_{III}}$, it is required to find the cumulative distribution function of Γ_{t_J}, where $\Gamma_{t_J} = \Gamma_{1_J} + \Gamma_{2_J}$. Thus, the cumulative distribution function associated with Γ_{t_J} is obtained as follows:

$$\begin{aligned} F_{\Gamma_{t_J}}(\gamma) &= \mathcal{P}r\big(\Gamma_{t_J} \leq \gamma\big) = \mathcal{P}r(X+Y \leq \gamma), \\ &= \int_0^{\gamma}\int_0^{\gamma-y} \frac{1}{\phi_{11}P_1\phi_{21}P_2} e^{-\frac{x}{\phi_{11}P_1}} e^{-\frac{y}{\phi_{21}P_2}}\, dx\, dy, \\ &= 1 - \frac{\phi_{11}P_1}{(\phi_{11}P_1 - \phi_{21}P_2)} e^{-\frac{\gamma}{\phi_{11}P_1}} \\ &\quad + \frac{\phi_{21}P_2}{(\phi_{11}P_1 - \phi_{21}P_2)} e^{-\frac{\gamma}{\phi_{21}P_2}}. \end{aligned} \tag{91}$$

Then the average BLER can be expressed as:

$$\begin{aligned} \overline{\epsilon_{III}} &= E[\epsilon_{III}], \\ &= \int_0^{\infty} f_{\Gamma_{t_J}}(\gamma) Q\left(\frac{\sqrt{N}(\log(1+\gamma) - R_1 - R_2)}{\sqrt{1 - \frac{1}{(1+\gamma)^2}}}\right) \mathrm{d}\gamma. \end{aligned} \tag{92}$$

By using the linear approximation for the Q-function as given in (104), and the cumulative distribution function of $\Gamma_{t,J}$ derived in (91), (92) is expressed as follows:

$$\begin{aligned} \overline{\epsilon_{III}} &= F_{\Gamma_{t_J}}\left(\alpha_3 - \frac{1}{2\beta_{3_{NG}}}\right) + \left(\frac{1}{2} + \alpha_3\beta_{3_{NG}}\right) \\ &\quad \left(F_{\Gamma_{t_J}}\left(\alpha_3 + \frac{1}{2\beta_{3_{NG}}}\right) - F_{\Gamma_{t_J}}\left(\alpha_3 - \frac{1}{2\beta_{3_{NG}}}\right)\right) \\ &\quad - \beta_{3_{NG}} \int_{\alpha_3 - \frac{1}{2\beta_{3_{NG}}}}^{\alpha_3 + \frac{1}{2\beta_{3_{NG}}}} \gamma f_{\Gamma_{t_J}}(\gamma)\ \mathrm{d}\gamma. \end{aligned} \tag{93}$$

By substituting (91) in (93) and with some algebraic manipulation, expression in (75) is obtained. By adding the terms in (73), (74), and (75), $\overline{\epsilon_J}$ can be obtained which is eventually used to evaluate $\mathcal{P}r(D_1^{\{1,2\}})$. In the following, the probability of successful decoding at Rx-2 is obtained.

Evaluation of $\mathcal{P}r(\mathcal{D}_2^{\{2\}})$*:* We know that

$$\mathcal{P}r\left(D_2^{\{2\}}\right) = 1 - \overline{\epsilon_{22_{NG}}}, \tag{94}$$

where

$$\epsilon_{22_{NG}} \approx Q\left(\frac{\sqrt{N}(\log(1+\gamma_{22}) - R_2}{\sqrt{V_{NG}(\gamma_{22})}}\right), \tag{95}$$

$$V_{NG} = 1 - \frac{1}{(1+\gamma_{22})^2}, \text{ and } \gamma_{22} = G_{22}P_2. \tag{96}$$

It can be seen that the expression of $\epsilon_{22_{NG}}$ in (95) is same as that of the expression of ϵ_{22_G} in (33), except that $V_G(\gamma_{22})$ is replaced by $V_{NG}(\gamma_{22})$, as Tx-2 uses non-Gaussian signaling. Hence, $\overline{\epsilon_{22_{NG}}}$ stated in (76) can be evaluated in the same way as that of $\overline{\epsilon_{22_G}}$, that has been derived in the case of SIC scheme.

b) When $Q_1 \neq 0$ *and* $Q_2 = 0$*:* The probability of successful decoding, in this case, is given by

$$\mathcal{P}r\left(D_1^{\{1\}}\right) = 1 - \overline{\epsilon_I}. \tag{97}$$

It can be seen that $\overline{\epsilon_I}$ corresponds to (73) and has been previously derived for the case where both the queues are active.

c) When $Q_1 = 0$ *and* $Q_2 \neq 0$*:* The probability of successful decoding, in this case, is given by

$$\mathcal{P}r\left(D_2^{\{2\}}\right) = 1 - \overline{\epsilon_{22_{NG}}}, \tag{98}$$

$$= 1 - E\big[\epsilon_{22_{NG}}\big]. \tag{99}$$

It can be seen that $\mathcal{P}r(D_2^{\{2\}})$ corresponds to (94) as Rx-2 does not experience any interference from Tx 1. ■

Remarks:

1) The result of Theorem 3 considers the product of error terms in both the decoding stages while evaluating the probability of successful decoding of the SIC scheme. From Fig. 3, it can be observed that at lower transmission rates, the probability of successful decoding is almost the same whether we ignore or consider the product of error terms. However, at higher transmission rates ($R \geq 0.6$), one can see that the probability of successful decoding is underestimated when the product of the error terms is ignored. When R increases beyond 1, the probability of successful decoding becomes zero, as the product of error terms is ignored. However, when the product of error terms is considered, this does not happen even if $R \geq 1$. Hence, it is required to consider the product of error terms for a high transmission rate. The product of error terms in the evaluation of average BLER gives accurate results compared to the work which has ignored the product of error terms [23], [29], [31], [32], [33].
2) One can use the results for a very strong interference regime in the case of the two-user AWGN IC [17] to obtain the achievable results for two-user Z-IC for specific channel conditions. This is left as a future extension of this work.
3) The probability of successful decoding obtained for various interference mitigation techniques does not consider path loss. The effect of path-loss can be taken into consideration by replacing $G_{ij} = |h_{ij}|^2$ with $|h_{ij}|^2 d_{ij}^{-\alpha_{ij}}$, where α_{ij} (d_{ij}) corresponds to the path-loss exponent (distance) between Tx-i and Rx-j ($i, j \in \{1, 2\}$).

V. AVERAGE DELAY AND AVERAGE AGE OF INFORMATION ANALYSIS

The stable throughput or the stability region does not capture the delay or latency associated with the communication. It is essential to understand how interference affects the timeliness of the data when devices are constrained to use short packets for communication, as in IoT or M2M scenarios.

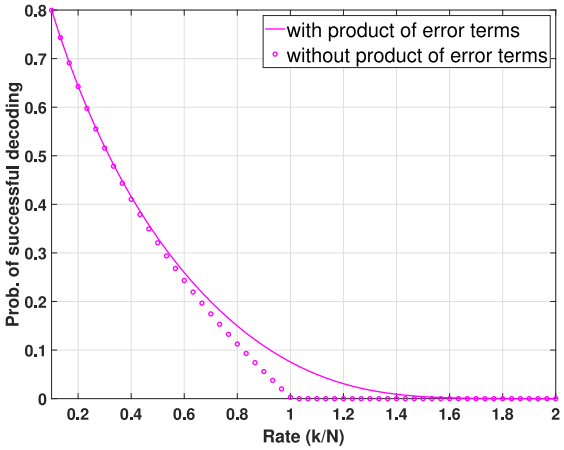

FIGURE 3. Probability of successful decoding vs rate: $P_1 = P_2 = 10W$, $N = 300$ channel uses, $\phi_{11} = \phi_{22} = 1$, $\phi_{21} = 0.5$.

To get more insight into this problem, the impact of various interference mitigation techniques on average delay and the AAoI are explored in this section. The AAoI metric fundamentally differs from delay and captures the freshness of information. As the queues are decoupled in the Z-IC, it is possible to characterize the AAoI and delay using the result in [43], [44], [45]. In the following, results related to Rx-1 (which experiences interference) are given, and one can obtain the results for Rx-2 similarly.

The average delay (Δ_1) and AAoI ($AAoI_1$) corresponding Tx-1 and Rx-1 are given by the following expressions [43], [44]:

$$\Delta_1 = \frac{1}{\mu_1} + \frac{1-\lambda_1}{\mu_1-\lambda_1}, \tag{100}$$

$$\text{and} \quad AAoI_1 = \frac{1}{\lambda_1} + \frac{1-\lambda_1}{\mu_1-\lambda_1} - \frac{\lambda_1}{\mu_1^2} + \frac{\lambda_1}{\mu_1}. \tag{101}$$

From (100) and (101), it can be seen that it is required to determine μ_1 to evaluate both delay and AAoI. The service probability corresponding to user 1 can be obtained from (16) as given below:

$$\mu_1 = \mathcal{P}r\left(D_1^{\{1\}}\right) + \frac{\lambda_2\left[\mathcal{P}r\left(D_1^{\{1,2\}}\right) - \mathcal{P}r\left(D_1^{\{1\}}\right)\right]}{\mathcal{P}r\left(D_2^{\{2\}}\right)}. \tag{102}$$

Hence, from (102), it can be seen that μ_1 not only depends on the mean arrival probability of Tx-2 (λ_2) but also on the scheme that is adopted at Rx-1 to mitigate interference. The different probabilities of successful decoding at the receiver can be obtained for the various interference mitigation schemes using the results developed in Section IV. Hence, one can use the service probability given in (102) to determine the average delay and AAoI for Tx-1 and Rx-1 where $(\lambda_1, \lambda_2) \in \mathcal{R}$, i.e., both the queues are stable. Recall that $\mathcal{R}$ corresponds to the stability region given in (4).

The AoI and delay performance of various decoding schemes depend on the probability of successful decoding of a packet at the receiver and arrival rate. The probability of successful decoding of the packet depends on the relative strength between signal and interference along with other parameters such as power budget at transmitter and blocklength.

VI. RESULTS AND DISCUSSION

This section presents results to illustrate the performance of various interference mitigation techniques when users are constrained to use short packets for communication. The average channel gain between Tx-i and Rx-i is fixed at $\phi_{ii} = 1$ for all the results. Two scenarios are considered by taking account of the relative strength between the interference and intended signal: (a) $\phi_{11} > \phi_{21}$ and (b) $\phi_{11} < \phi_{21}$.

A. PROBABILITY OF SUCCESSFUL DECODING AND AVERAGE BLER

In Fig. 4, probability of successful decoding ($\mathcal{P}r(D_1^{\{1,2\}})$) for various interference mitigation schemes stated in Theorems 2-4 are plotted against N, when both the queues are active. The simulation results for various schemes are obtained by averaging over the corresponding instantaneous error expressions in Theorems 2-4 over 10^6 channel realizations. For the TIN scheme, the instantaneous error in (29) is averaged over 10^6 channel realizations. To obtain the simulation result for the probability of successful decoding in the case of SIC scheme, the instantaneous error terms in (55), and (57) are averaged over 10^6 channel realizations. Similarly, for the joint decoding scheme, the RHS of different error terms in (78) are averaged over 10^6 various channel realizations. The results presented in the framework of finite block length coding are accurate when the block-length is in the order of 100 channel uses.

The number of information bits and power at both the transmitters are set at $k_1 = k_2 = 30$ nats and $P_1 = P_2 = 50W$, respectively. The probability of successful decoding for all the schemes increases with block-length N. From Fig. 4(a) ($\phi_{11} = \phi_{22} = 1$ and $\phi_{21} = 0.5$), it is interesting to note that the joint decoding scheme performs better in comparison to other schemes even when $\phi_{21} < \phi_{11}$. The SIC scheme achieves the lowest probability of successful decoding as the interfering user's average channel gain is weak compared to the intended user's average channel gain. Due to this, the average BLER in the first stage of the SIC scheme is higher, affecting the decoding of the intended message in the second stage. To illustrate the error performance of various decoding schemes, average BLER ($1 - \mathcal{P}r(D_1^{\{1,2\}})$) at Rx-1 (when both the queues are active) is plotted against block length N in Fig. 5. The joint decoding scheme can achieve low average BLER even with short block-length compared to other schemes but at the cost of increased complexity at the receiver.

In Fig. 4(b), the average channel gain corresponding to the interfering link is stronger than the direct link ($\phi_{11} = \phi_{22} = 1$ and $\phi_{21} = 1.5$). In this case, the SIC scheme performs better than the TIN scheme for a larger

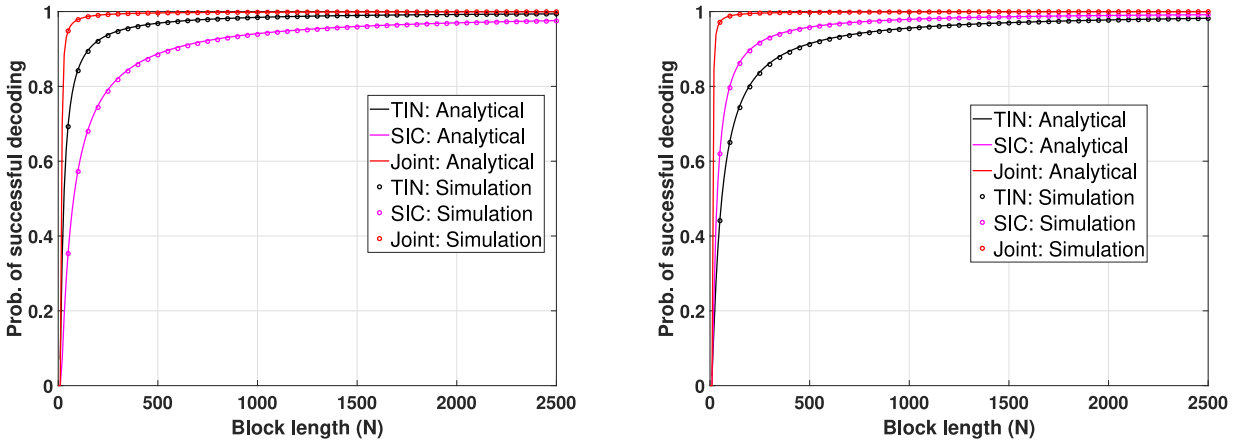

(a) $\phi_{21} = 0.5$. (b) $\phi_{21} = 1.5$.

FIGURE 4. Probability of successful decoding at Rx-1 versus blocklength N (channel uses): $P_1 = P_2 = 50$W, $k_1 = k_2 = 30$ nats, and $\phi_{11} = \phi_{22} = 1$.

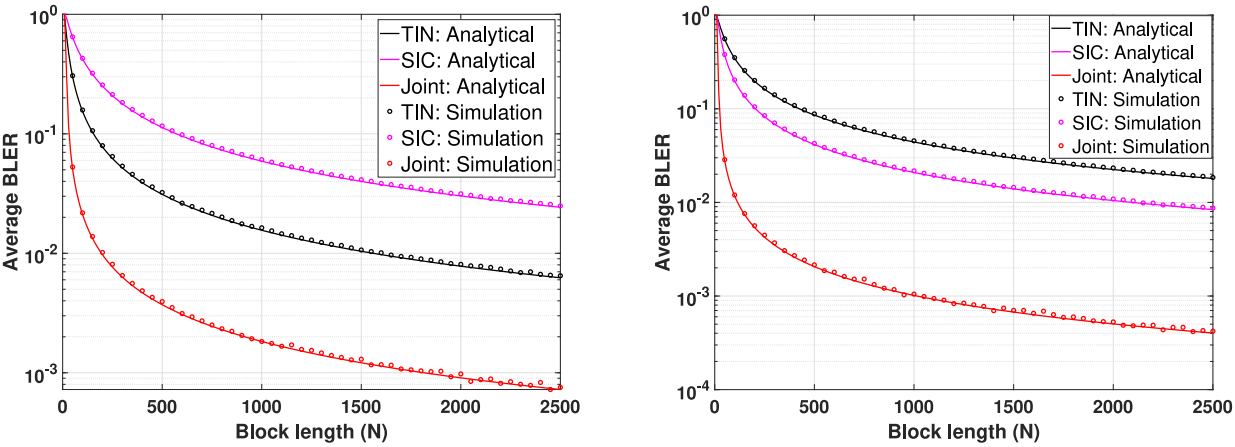

(a) $\phi_{21} = 0.5$. (b) $\phi_{21} = 1.5$.

FIGURE 5. Average BLER at Rx-1 versus blocklength N (channel uses): $P_1 = P_2 = 50$W, $k_1 = k_2 = 30$ nats, and $\phi_{11} = \phi_{22} = 1$.

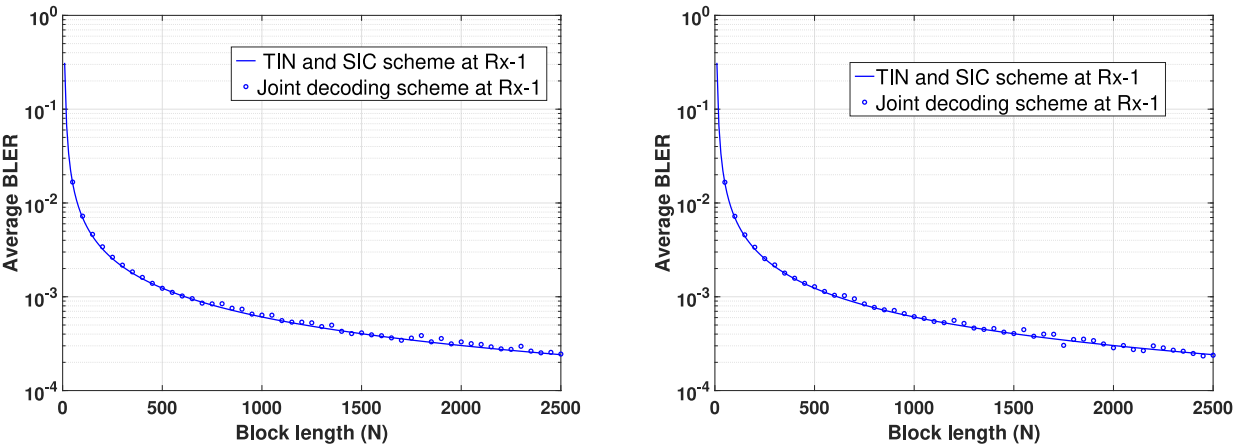

(a) $\phi_{21} = 0.5$. (b) $\phi_{21} = 1.5$.

FIGURE 6. Average BLER at Rx-2 versus blocklength N (channel uses): $P_1 = P_2 = 50$W, $k_1 = k_2 = 30$ nats, and $\phi_{11} = \phi_{22} = 1$.

range of N as $\phi_{21} > \phi_{11}$ in comparison to Fig. 4(a). The joint decoding scheme performs the best among all the considered schemes. It can be noticed that the joint decoding scheme can achieve average BLER in the order of 10^{-3} even when $N = 1000$ channel uses as compared to other schemes (See Fig. 5(b)).

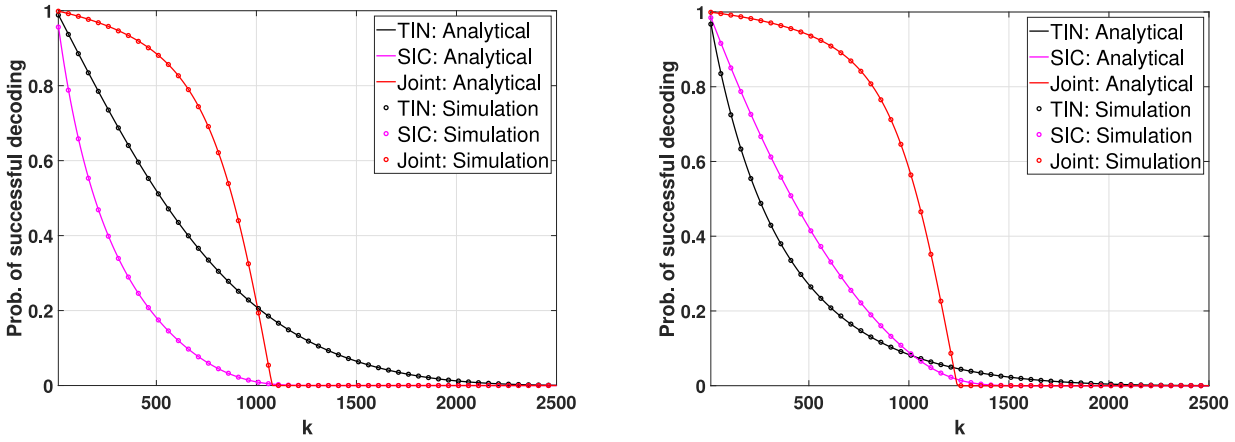

(a) $\phi_{21} = 0.5$. (b) $\phi_{21} = 1.5$.

FIGURE 7. Probability of successful decoding at Rx-1 versus number of information bits k (nats): $P_1 = P_2 = 50$W, $N = 500$ channel uses, and $\phi_{11} = \phi_{22} = 1$.

In Fig. 6, the average BLER for Rx-2 is plotted when different decoding schemes are used at Rx-1. Recall that for the TIN and the SIC scheme (See Theorems 2-3), Tx-2 uses Gaussian signalling, whereas for the joint decoding scheme (See Theorem 4), Tx-2 uses non-Gaussian signalling. Hence, the average BLER expression is the same for Rx-2 in the case of TIN and SIC schemes. One can notice that the average BLER in the case of Rx-2 is less compared to Rx-1 as Rx-2 does not experience any interference. It is also found that the average BLER for different cases is almost the same, although the non-Gaussian signalling scheme achieves lower dispersion compared to Gaussian signalling.

In Fig. 7, the probability of successful decoding $\mathcal{P}r(D_1^{\{1,2\}})$ at Rx-1 is plotted versus the number of information nats ($k_i = k$) for a given block-length $N = 500$ channel uses, when both the queues are active. From Fig. 7(a), it is interesting to note that the joint decoding scheme gives the best performance, even when the average channel gain of the interfering user is less than the average channel gain of the direct link for a wide range of k. However, when k increases beyond a specific value (around 1000 nats), the TIN scheme performs best among the considered schemes. This is because the error in decoding the messages increases with an increase in the rate ($R_i = \frac{k_i}{N}$), as Rx-1 needs to decode both the messages in joint decoding. However, in the TIN scheme, Rx-1 does not need to decode the message of the unintended user. From Fig. 7(b), one can also observe that the joint decoding scheme outperforms other schemes for a broader range of k when compared to Fig. 7(a), as $\phi_{21} > \phi_{11}$. As the interfering user's average channel gain is stronger than the intended user's average channel gain, Rx-1 can support a higher rate from both users with less error. One can also notice from Fig. 7(b) that even when $\phi_{21} > \phi_{11}$, the TIN scheme performs better in comparison to the SIC scheme for high values of k, as Rx-1 does not need to decode the interference in case of TIN scheme.

B. STABILITY REGION

In Fig. 8, the stability region of Z-IC in Theorem 1 is plotted for $P_1 = P_2 = 50$W, $N = 500$ channel uses, and $k_1 = k_2 = 300$ nats. It can be seen from Fig. 8(a) ($\phi_{11} > \phi_{21}$) that there is no single scheme that can achieve the largest stability region. From Fig. 8(a), one can notice that when user 1 supports a maximum arrival rate of 0.97 packets/slot, it is not possible to support any packet at user 2. When the TIN scheme is used at Rx-1, Tx-2 can support an arrival rate of 0.97 packets/slot, but at the cost of a reduced arrival rate that can be supported at Tx-1 in comparison to SIC scheme. When the arrival probability at Tx-1 increases beyond 0.7 packet/slot, it is preferable to use a joint decoding scheme at Rx-1, as it allows both the users to support a higher arrival rate without violating the stability criteria in comparison to other schemes. This gain comes from decoding the interference caused by Tx-2 at Rx-1. The SIC scheme is not able to provide a larger stability region, as the decoding error in the first stage of SIC propagates to the next stage of decoding at Rx-1, as $\phi_{21} < \phi_{11}$.

When $\phi_{21} > \phi_{11}$, the joint decoding scheme provides the largest stability region, and both the users can support a maximum arrival rate close to 1 packet/slot (See Fig. 8(b)). The stability region corresponding to the SIC scheme is larger than the TIN scheme, which contrasts the result in Fig. 8(a).

In Fig. 9, the stability region is plotted for the case where both the users transmit at a lower rate ($k_1 = k_2 = 30$ *nats*) as compared to the result in Fig. 8. From Fig. 9(a), it can be observed that stability regions corresponding to TIN and joint decoding schemes are almost similar at lower transmission rates. Similar observations can be made from Fig. 9(b).

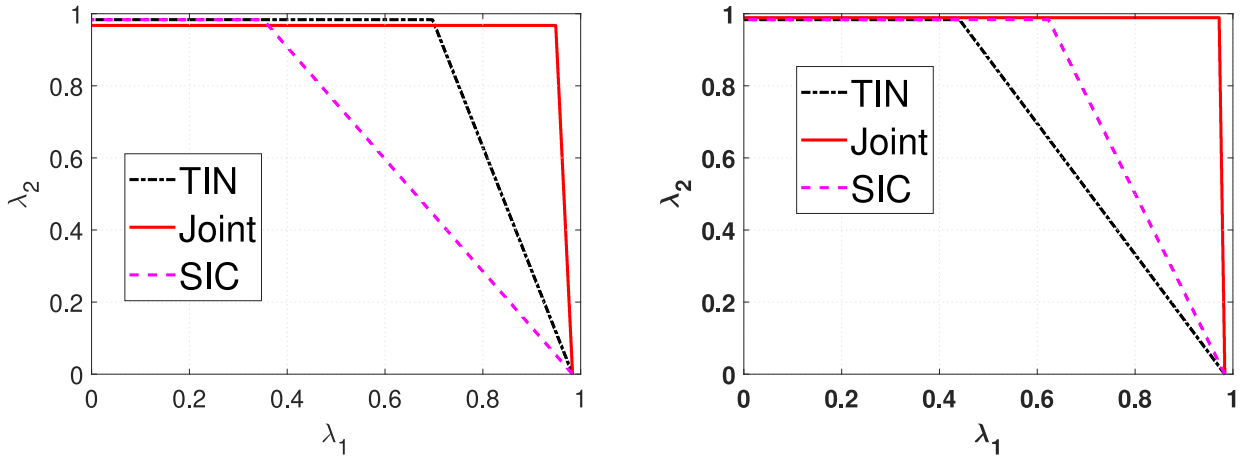

(a) $\phi_{21} = 0.5$ (b) $\phi_{21} = 1.5$

FIGURE 8. Stability region: $P_1 = P_2 = 50$W, $N = 500$ channel uses, $k_1 = k_2 = 300$ nats, and $\phi_{11} = \phi_{22} = 1$.

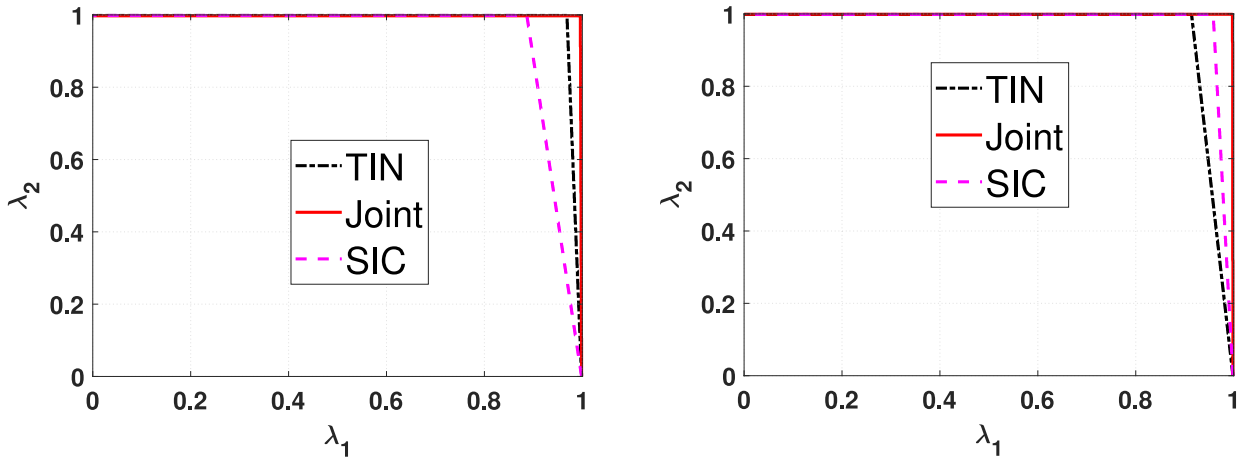

(a) $\phi_{21} = 0.5$ (b) $\phi_{21} = 1.5$

FIGURE 9. Stability region: $P_1 = P_2 = 50$W, $N = 500$ channel uses, $k_1 = k_2 = 30$ nats, and $\phi_{11} = \phi_{22} = 1$.

C. AVERAGE DELAY AND AAOI

In Figs. 10 ($\phi_{11} > \phi_{21}$) and 12 ($\phi_{11} < \phi_{21}$), average delay in (100) corresponding to different interference mitigation schemes at Tx-1 is plotted as a function of arrival probability λ_1 where $(\lambda_1, \lambda_2) \in \mathcal{R}$ in (4). The impact of the arrival rate at Tx-2 (λ_2) and the relative strength between the intended signal and interference is also illustrated. Note that average delay or AAoI depends on μ_1 and λ_1. The service probability μ_1 depends on the arrival rate at Tx-2, the decoding scheme used at Rx-1, and the underlying channel condition. The different probabilities of successful decoding involved in (102) are obtained for various interference management schemes as mentioned in Section IV. From Figs. 10 and 12, it can be observed that when the arrival rate at user one increases, the average delay gradually increases for all the schemes. The TIN scheme ensures lower delay compared to the SIC scheme when $\phi_{21} < \phi_{11}$ (See Fig. 10). When $\phi_{21} > \phi_{11}$, the SIC scheme provides a smaller delay than the TIN scheme (See Fig. 12). However, the joint-decoding scheme provides the lowest delay among all the considered schemes.

Moreover, it can be seen from Figs. 10(a) and 10(b) that as the arrival rate at Tx-2 (λ_2) increases, the delay increases for both SIC and TIN schemes, as the interference increases with an increase in the arrival rate at Tx-2. However, joint decoding provides almost similar delay performance even when λ_2 increases. A similar phenomenon can be observed in Figs. 12(a) and 12(b).

In Figs. 11 and 13, average AoI at Tx-1 as stated in (101) is plotted as a function of λ_1 for different arrival probabilities at Tx-2 as well as for different relative strength between the intended signal and interference. When the arrival probability is low at the Tx-1, AAoI is high, as the receiver is not getting fresh updates. As the arrival probability at user-1 increases, the AAoI decreases as the receiver gets enough updates. However, after a certain arrival probability, AAoI increases with an increase in the arrival probability due to the increase in the queuing delay at the transmitter. It can

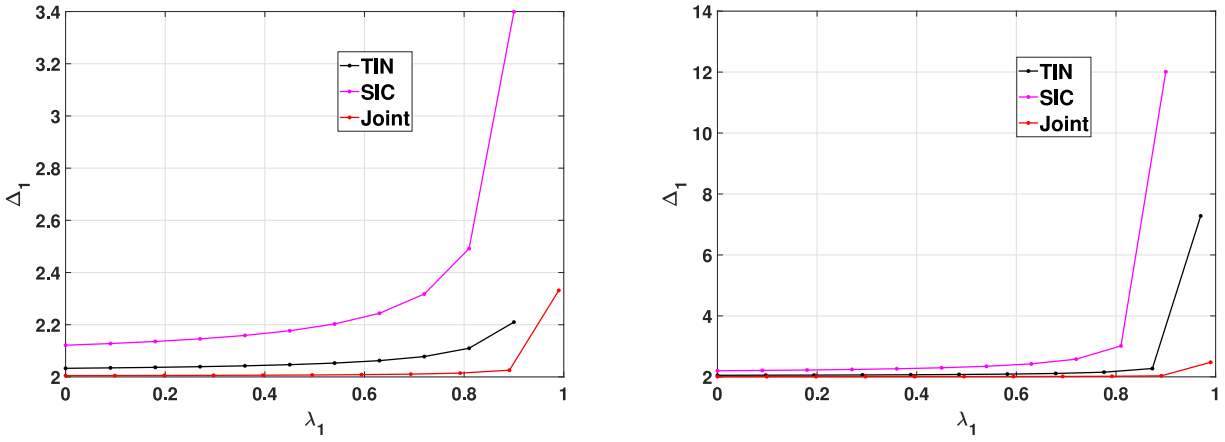

(a) $\phi_{21} = 0.5,\ \lambda_2 = 0.5.$ (b) $\phi_{21} = 0.5\ \lambda_2 = 0.8.$

FIGURE 10. Delay at user-1 versus arrival rate at user-1 (λ_1) for two different values of λ_2: $P_1 = P_2 = 50$W, $\phi_{11} = \phi_{22} = 1$, $\phi_{21} = 0.5$, $k_1 = k_2 = 30$ nats, and $N = 500$ channel uses.

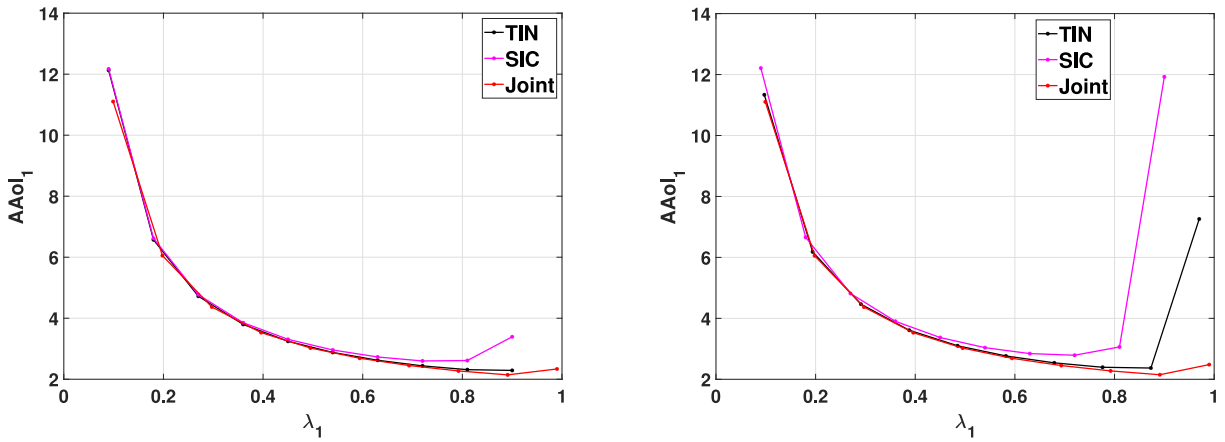

(a) $\phi_{21} = 0.5,\ \lambda_2 = 0.5.$ (b) $\phi_{21} = 0.5\ \lambda_2 = 0.8.$

FIGURE 11. AAoI at user-1 versus arrival rate at user-1 (λ_1) for two different values of λ_2: $P_1 = P_2 = 50$W, $\phi_{11} = \phi_{22} = 1$, $\phi_{21} = 0.5$, $k_1 = k_2 = 30$ nats, and $N = 500$ channel uses.

also be observed that joint decoding can achieve low AAoI and low average delay simultaneously.

Moreover, it can be seen from Figs. 11(a) and 11(b) that as the arrival rate at Tx-2 (λ_2) increases, AAoI increases for both SIC and TIN schemes. This is due to an increase in the interference with an increase in λ_2 at Tx-2. However, it can be seen that joint decoding provides almost similar AAoI even when λ_2 increases. Similar behaviour can be observed in Figs. 13(a) and 13(b).

From the results, it can be noticed that when the average channel gain of the interfering user is less than the average channel gain of the intended user, the receiver can employ the TIN scheme as it can support high stable throughput, low delay, and low AAoI in comparison to the SIC scheme. Moreover, when it is required to support a high arrival rate at both users simultaneously, it is preferred to use a joint decoding scheme at Rx-1, as it can provide low delay and low AAoI. However, these benefits come at the cost of increased complexity in joint decoding. When the average channel gain of the interfering user is less than the average channel gain of the intended user, a joint decoding scheme can be used as it can provide significant improvement in throughput and latency compared to other schemes, even though it has high implementation complexity.

D. RESULTS WITH DIFFERENT POWER CONSIDERATIONS AT THE USERS

This section presents results to investigate the performance of different interference mitigation schemes under different power budget assumptions at the transmitters. For all the results, it is assumed that $P_1 = 50W,\ P_2 = 130W,\ \phi_{11} = \phi_{22} = 1,$ and $\phi_{21} = 0.5$.

In Fig. 14, the probability of successful decoding at Rx-1 ($\mathcal{P}r(D_1^{\{1,2\}})$) is plotted as a function of block length N for different decoding schemes when both the queues are active. Interestingly, even in the weak interference regime, the SIC scheme performs better than the TIN scheme. As Tx-2 has a high-power budget compared to Tx-1, the error in the first stage of decoding reduces, where the message of Tx-1 is treated as noise. The reduced error in the first stage of

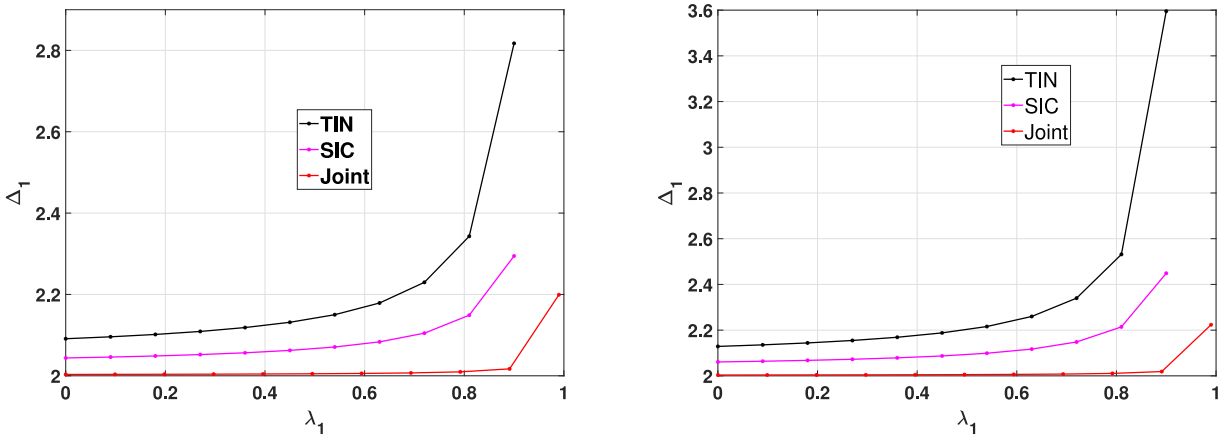

(a) $\phi_{21} = 1.5$ $\lambda_2 = 0.5$. (b) $\phi_{21} = 1.5$ $\lambda_2 = 0.7$.

FIGURE 12. Delay at user-1 versus arrival rate at user-1 (λ_1) for two different values of λ_2: $P_1 = P_2 = 50$W, $\phi_{11} = \phi_{22} = 1$, $\phi_{21} = 1.5$, $k_1 = k_2 = 30$ nats, and $N = 500$ channel uses.

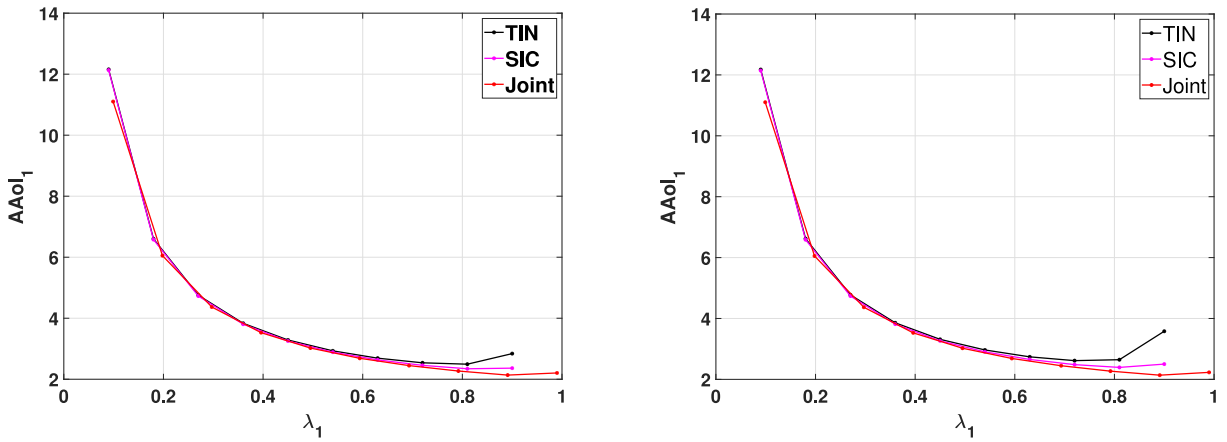

(a) $\phi_{21} = 1.5$ $\lambda_2 = 0.5$. (b) $\phi_{21} = 1.5$ $\lambda_2 = 0.7$.

FIGURE 13. AAoI at user-1 versus arrival rate at user-1 (λ_1) for two different values of λ_2: $P_1 = P_2 = 50$W, $\phi_{11} = \phi_{22} = 1$, $\phi_{21} = 1.5$, $k_1 = k_2 = 30$ nats, and $N = 500$ channel uses.

decoding improves the overall error performance of the SIC scheme. Due to this, the stability region corresponding to the SIC scheme is larger than the TIN scheme (See Fig. 15). When the same power budget is used at both transmitters, the TIN scheme simultaneously supports a larger arrival rate for both users than the SIC scheme (See Fig. 9(a)). The stability region corresponding to the joint decoding scheme is the largest when compared to other schemes, as the joint decoding scheme has the highest probability of successful decoding compared to other schemes.

In Fig. 16, the average delay and AAoI of user-1 are plotted as a function of λ_1. The SIC scheme ensures lower average delay and average AoI as compared to the TIN scheme even when $\phi_{21} < \phi_{11}$. The joint decoding scheme provides better AAoI and delay performance and supports a higher arrival rate at Tx-1 compared to the other schemes.

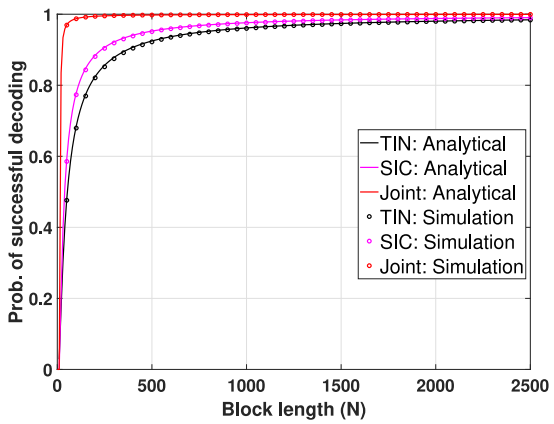

FIGURE 14. Probability of successful decoding at Rx-1 versus blocklength N channel uses: $P_1 = 50$W, $P_2 = 130$W, $k_1 = k_2 = 30$ nats, $\phi_{11} = \phi_{22} = 1$, and $\phi_{21} = 0.5$.

VII. CONCLUSION

This work characterizes the stability region of the two-user Rayleigh fading Z-IC, which has not been explored in the existing literature. The evaluation of the stability region involves the characterization of the probability of successful decoding at the receivers. The finite block length information

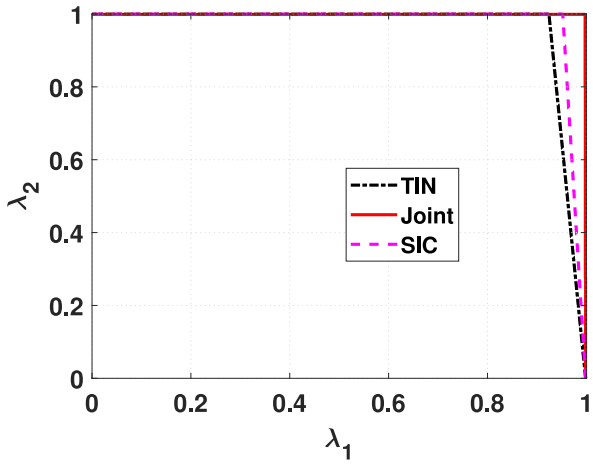

FIGURE 15. Stability region: $P_1 = 50$W, $P_2 = 130$W, $N = 500$ channel uses, $k_1 = k_2 = 30$ nats, $\phi_{11} = \phi_{22} = 1$, and $\phi_{21} = 0.5$.

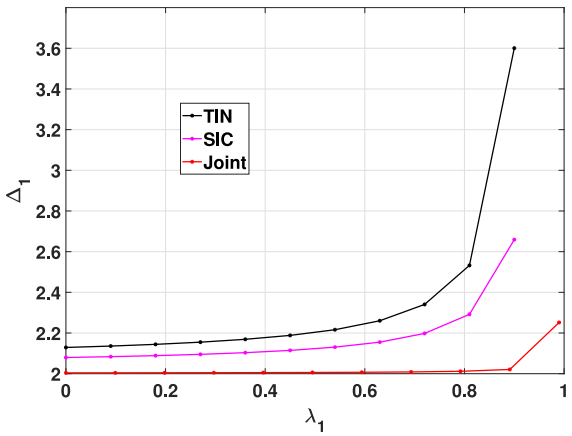

(a) Delay at user-1 vs λ_1 for $\lambda_2 = 0.8$

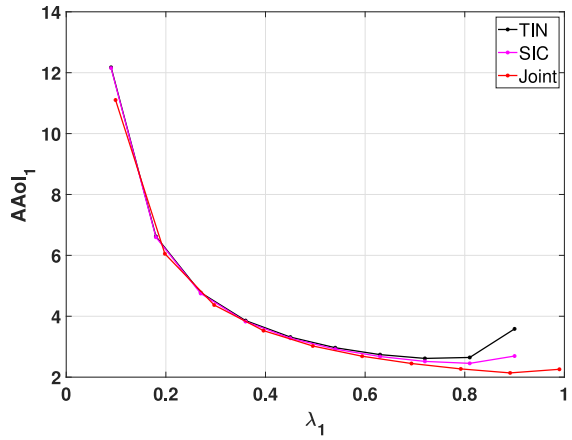

(b) AAoI of user-1 vs λ_1 for $\lambda_2 = 0.8$

FIGURE 16. Delay and AAoI of user-1: $P_1 = 50$W, $P_2 = 130$W, $\phi_{11} = \phi_{22} = 1$, $\phi_{21} = 0.5$, $k_1 = k_2 = 30$ nats, and $N = 500$ channel uses.

theory framework was used to obtain an approximate closed-form expression for the probability of successful decoding corresponding to various decoding schemes at the receiver. The performance of various decoding schemes depends not only on the channel conditions but also on the arrival rate at the user, packet length, and rate associated with the user. The developed results further help to explore the interplay between packet length, average delay, and AAoI in the case of interference-limited scenarios.

APPENDIX A
DERIVATION OF $\overline{\epsilon_{TIN}}$ IN THEOREM 2

Linearization technique [46] is used to approximate the Q-function in (29), at point $x = \alpha$ as given below:

$$Q\left(\frac{\sqrt{N}(\log(1+x)-R)}{\sqrt{V_{NG}(x)}}\right) \simeq U_{NG}(x), \text{ where} \tag{103}$$

$$U_{NG}(x) = \begin{cases} 1, & x \le \alpha - \frac{1}{2\beta_{NG}}, \\ \rho_{NG} - \beta_{NG}x, & x \in \left[\alpha - \frac{1}{2\beta_{NG}}, \alpha + \frac{1}{2\beta_{NG}}\right], \\ 0, & x \ge \alpha + \frac{1}{2\beta_{NG}}. \end{cases} \tag{104}$$

$$\alpha \triangleq e^R - 1, \quad \rho_{NG} \triangleq \frac{1}{2} + \alpha\beta_{NG}, \text{ and}$$

$$\beta_{NG} \triangleq -\left.\frac{\partial\left(Q\left(\frac{\sqrt{N}(\log(1+x)-R)}{\sqrt{1-\frac{1}{(1+x)^2}}}\right)\right)}{\partial x}\right|_{x=\alpha} = \sqrt{\frac{N}{2\pi(e^{2R}-1)}}.$$

The cumulative distribution function (CDF) associated with SINR ($\Gamma_{1,TIN}$) at Rx-1 is given by the following expression:

$$\begin{aligned} F_{\Gamma_{1,TIN}}(x) &= Pr\left(\frac{G_{11}P_1}{1+G_{21}P_2} \le x\right), \\ &= \int_0^\infty Pr\left(G_{11} \le \frac{x(1+P_2y)}{P_1}\right) f_{G_{21}}(y)\, dy, \\ &= \int_0^\infty \left(1 - e^{-\frac{x(1+P_2y)}{\phi_{11}P_1}}\right)\frac{1}{\phi_{21}} e^{-\frac{y}{\phi_{21}}}\, dy, \\ &= 1 - e^{-\frac{x}{\phi_{11}P_1}}\left(\frac{1}{1+\frac{\phi_{21}P_2}{\phi_{11}P_1}x}\right), \quad x \ge 0. \end{aligned} \tag{105}$$

Using (31), (103) and (105), the average BLER ($\overline{\epsilon_{TIN}}$) can be evaluated as follows

$$\begin{aligned} \overline{\epsilon_{TIN}} &= \int_0^\infty f_{\Gamma_{1,TIN}}(\gamma_1) Q\left(\frac{\sqrt{N}(\log(1+\gamma_1)-R_1)}{\sqrt{1-\frac{1}{(1+\gamma_1)^2}}}\right) d\gamma_1, \\ &\approx \int_0^{\alpha_1 - \frac{1}{2\beta_{1_{NG}}}} f_{\Gamma_{1,TIN}}(\gamma_1).(1) d\gamma_1 \\ &\quad + \int_{\alpha_1 - \frac{1}{2\beta_{1_{NG}}}}^{\alpha_1 + \frac{1}{2\beta_{1_{NG}}}} f_{\Gamma_{1,TIN}}(\gamma_1)\left(\rho_{1_{NG}} - \beta_{1_{NG}}\gamma_1\right) d\gamma_1, \\ &\approx \int_0^{\alpha_1 - \frac{1}{2\beta_{1_{NG}}}} f_{\Gamma_{1,TIN}}(\gamma_1).(1) d\gamma_1 + \\ &\quad \int_{\alpha_1 - \frac{1}{2\beta_{1_{NG}}}}^{\alpha_1 + \frac{1}{2\beta_{1_{NG}}}} f_{\Gamma_{1,TIN}}(\gamma_1)\left(\frac{1}{2} + \beta_{1_{NG}}(\alpha_1 - \gamma_1)\right) d\gamma_1, \\ &= F_{\Gamma_{1,TIN}}\left(\alpha_1 - \frac{1}{2\beta_{1_{NG}}}\right) + \left(\frac{1}{2} + \alpha_1\beta_{1_{NG}}\right) \end{aligned}$$

$$\left(F_{\Gamma_{1,TIN}}\left(\alpha_1+\frac{1}{2\beta_{1_{NG}}}\right)-F_{\Gamma_{1,TIN}}\left(\alpha_1-\frac{1}{2\beta_{1_{NG}}}\right)\right)$$
$$-\beta_{1_{NG}}\int_{\alpha_1-\frac{1}{2\beta_{1_{NG}}}}^{\alpha_1+\frac{1}{2\beta_{1_{NG}}}}\gamma_1 f_{\Gamma_{1,TIN}}(\gamma_1)d\gamma_1,$$
$$=1-\frac{e^{-\frac{\left(\alpha_1-\frac{1}{2\beta_{1_{NG}}}\right)}{\phi_{11}P_1}}}{1+\frac{\phi_{21}P_2}{\phi_{11}P_1}\left(\alpha_1-\frac{1}{2\beta_{1_{NG}}}\right)}+\left(\frac{1}{2}+\alpha_1\beta_{1_{NG}}\right)$$
$$\left(\frac{e^{-\frac{\left(\alpha_1-\frac{1}{2\beta_{1_{NG}}}\right)}{P_1\phi_{11}}}}{1+\frac{\phi_{21}P_2}{\phi_{11}P_1}\left(\alpha_1-\frac{1}{2\beta_{1_{NG}}}\right)}-\frac{e^{-\frac{\left(\alpha_1+\frac{1}{2\beta_{1_{NG}}}\right)}{P_1\phi_{11}}}}{1+\frac{\phi_{21}P_2}{\phi_{11}P_1}\left(\alpha_1+\frac{1}{2\beta_{1_{NG}}}\right)}\right)$$
$$-\beta_{1_{NG}}\left(\left(\alpha_1-\frac{1}{2\beta_{1_{NG}}}\right)\left(\frac{e^{-\frac{\left(\alpha_1-\frac{1}{2\beta_{1_{NG}}}\right)}{P_1\phi_{11}}}}{1+\frac{\phi_{21}P_2}{\phi_{11}P_1}\left(\alpha_1-\frac{1}{2\beta_{1_{NG}}}\right)}\right)\right. \quad (106)$$
$$-\left(\alpha_1+\frac{1}{2\beta_{1_{NG}}}\right)\left(\frac{e^{-\frac{\left(\alpha_1+\frac{1}{2\beta_{1_{NG}}}\right)}{P_1\phi_{11}}}}{1+\frac{\phi_{21}P_2}{\phi_{11}P_1}\left(\alpha_1+\frac{1}{2\beta_{1_{NG}}}\right)}\right)$$
$$\left.+\int_{\alpha_1-\frac{1}{2\beta_{1_{NG}}}}^{\alpha_1+\frac{1}{2\beta_{1_{NG}}}}\frac{e^{-\frac{\gamma_1}{\phi_{11}P_1}}}{1+\frac{\phi_{21}P_2}{\phi_{11}P_1}\gamma_1}d\gamma_1\right),$$
$$=1-\beta_{1_{NG}}\int_{\alpha_1-\frac{1}{2\beta_{1_{NG}}}}^{\alpha_1+\frac{1}{2\beta_{1_{NG}}}}\frac{e^{-\frac{\gamma_1}{\phi_{11}P_1}}}{1+\frac{\phi_{21}P_2}{\phi_{11}P_1}\gamma_1}d\gamma_1. \quad (107)$$

Using the definition of exponential integral defined in (26) in (107), the average error at Rx-1 given in (24) is obtained.

APPENDIX B
DERIVATION OF $E[\epsilon_{21}\epsilon_{11_G}]$ IN THEOREM 3

From (55), (57), and (60), $\overline{\epsilon_{21}\epsilon_{11_G}}$ in (59) is further simplified as shown at the bottom of next page, where δ_1^l, δ_1^u, δ_2^l, and δ_2^u are defined in (50), shown at the bottom of the p. 9. By using the linear approximation of $U_G(\gamma_{21})$ as defined in (37) and $f(\gamma_{21}|\gamma_{11})$ obtained in (61), the terms I_1 and I_2 simplify to the following:

$$I_1\approx\int_0^{\delta_2^l}1.f(\gamma_{21}|\gamma_{11})\,d\gamma_{21}=\left(1-e^{-\frac{\delta_2^l(1+\gamma_{11})}{\phi_{21}P_2}}\right), \quad (110)$$

$$I_2\approx\int_{\delta_2^l}^{\delta_2^u}\left(\rho_{2_G}-\beta_{2_G}\gamma_{21}\right)f(\gamma_{21}|\gamma_{11})\,d\gamma_{21},$$
$$=\int_{\delta_2^l}^{\delta_2^u}\rho_{2_G}\left(\frac{1+\gamma_{11}}{P_2\phi_{21}}\right)e^{-\frac{1}{\phi_{21}}\left(\frac{\gamma_{21}(1+\gamma_{11})}{P_2}\right)}d\gamma_{21}$$
$$-\int_{\delta_2^l}^{\delta_2^u}\beta_{2_G}\gamma_{21}\left(\frac{1+\gamma_{11}}{P_2\phi_{21}}\right)e^{-\frac{1}{\phi_{21}}\left(\frac{\gamma_{21}(1+\gamma_{11})}{P_2}\right)}d\gamma_{21},$$
$$=\left[\rho_{2_G}\left(e^{-\frac{\delta_2^l(1+\gamma_{11})}{\phi_{21}P_2}}-e^{-\frac{\delta_2^u(1+\gamma_{11})}{\phi_{21}P_2}}\right)\right.$$
$$-\beta_{2_G}\left(\delta_2^l e^{-\delta_2^l\frac{(1+\gamma_{11})}{\phi_{21}P_2}}-\delta_2^u e^{-\delta_2^u\frac{(1+\gamma_{11})}{\phi_{21}P_2}}\right)$$
$$\left.+\frac{\beta_{2_G}\phi_{21}P_2}{(1+\gamma_{11})}\left(e^{-\frac{\delta_2^u(1+\gamma_{11})}{\phi_{21}P_2}}-e^{-\frac{\delta_2^l(1+\gamma_{11})}{\phi_{21}P_2}}\right)\right], \quad (111)$$

where ρ_{2_G} is defined in (50). The term I in (109), shown at the bottom of the next page is evaluated using (110) and (111), and after some simplifications, the following is obtained:

$$I=I_1+I_2,$$
$$=1+\frac{\beta_{2_G}\phi_{21}P_2}{(1+\gamma_{11})}\left(e^{-\frac{\delta_2^u(1+\gamma_{11})}{\phi_{21}P_2}}-e^{-\frac{\delta_2^l(1+\gamma_{11})}{\phi_{21}P_2}}\right). \quad (112)$$

By using I obtained in (112), and the linear approximation of $U_G(\gamma_{11})$ defined in (37), (109) is further simplified as follows:

$$\overline{\epsilon_{21}\epsilon_{11_G}}=\int_0^{\delta_1^u}I.U_G(\gamma_{11})f(\gamma_{11})\,d\gamma_{11},$$
$$\approx\int_0^{\delta_1^l}I.1.f(\gamma_{11})\,d\gamma_{11}$$
$$+\int_{\delta_1^l}^{\delta_1^u}I.\left(\rho_{1_G}-\beta_{1_G}\gamma_{11}\right)f(\gamma_{11})\,d\gamma_{11},$$
$$=\underbrace{\int_0^{\delta_1^l}I.f(\gamma_{11})\,d\gamma_{11}}_{\triangleq I_3}+\underbrace{\int_{\delta_1^l}^{\delta_1^u}I.\rho_{1_G}f(\gamma_{11})\,d\gamma_{11}}_{\triangleq I_4}$$
$$\underbrace{-\int_{\delta_1^l}^{\delta_1^u}I.\beta_{1_G}\gamma_{11}f(\gamma_{11})\,d\gamma_{11}}_{\triangleq I_5},$$
$$=I_3+I_4-I_5. \quad (113)$$

By making use of I and $f(\gamma_{11})$ obtained in (112) and (62) respectively, I_3 in (113) is evaluated as follows:

$$I_3=\int_0^{\delta_1^l}\left(1+\frac{\beta_{2_G}\phi_{21}P_2}{(1+\gamma_{11})}\left(e^{-\frac{\delta_2^u(1+\gamma_{11})}{\phi_{21}P_2}}\right.\right.$$
$$\left.\left.-e^{-\frac{\delta_2^l(1+\gamma_{11})}{\phi_{21}P_2}}\right)\right)f(\gamma_{11})\,d\gamma_{11},$$
$$=\int_0^{\delta_1^l}f(\gamma_{11})\,d\gamma_{11}+\frac{\beta_{2_G}\phi_{21}P_2}{\phi_{11}P_1}$$
$$\left(\int_0^{\delta_1^l}\frac{e^{-\frac{\gamma_{11}}{\phi_{11}P_1}}}{(1+\gamma_{11})}\left(e^{-\frac{\delta_2^u(1+\gamma_{11})}{\phi_{21}P_2}}-e^{-\frac{\delta_2^l(1+\gamma_{11})}{\phi_{21}P_2}}\right)d\gamma_{11}\right),$$
$$=\left(1-e^{-\frac{\delta_1^l}{\phi_{11}P_1}}\right)$$
$$+\frac{\beta_{2_G}\phi_{21}P_2}{\phi_{11}P_1}\left(\int_0^{\delta_1^l}\frac{e^{-\frac{\delta_2^u}{\phi_{21}P_2}}e^{-\gamma_{11}h(\delta_2^u)}}{1+\gamma_{11}}d\gamma_{11}\right.$$
$$\left.-\int_0^{\delta_1^l}\frac{e^{-\frac{\delta_2^l}{\phi_{21}P_2}}e^{-\gamma_{11}h(\delta_2^l)}}{1+\gamma_{11}}d\gamma_{11}\right),$$

$$= \left(1 - e^{-\frac{\delta_1^l}{\phi_{11}P_1}}\right) + \frac{\beta_{2_G}\phi_{21}P_2 e^{\frac{1}{\phi_{11}P_1}}}{\phi_{11}P_1} \times \left[Ei\left(-\left(1+\delta_1^l\right)h\left(\delta_2^u\right)\right) - Ei\left(-h\left(\delta_2^u\right)\right) - Ei\left(-\left(1+\delta_1^l\right)h\left(\delta_2^l\right)\right) + Ei\left(-h\left(\delta_2^l\right)\right)\right], \quad (114)$$

where $h(\delta_2^l)$ and $h(\delta_2^u)$ are defined in (51), shown at the bottom of the p. 9 and $Ei(x)$ is defined in (26). I_4 specified in (113) can be obtained by following the same procedure used in evaluation of I_3 and is given by the following expression:

$$I_4 = \rho_{1_G}\left(e^{-\frac{\delta_1^l}{\phi_{11}P_1}} - e^{-\frac{\delta_1^u}{\phi_{11}P_1}}\right) + \frac{\rho_{1_G}\beta_{2_G}\phi_{21}P_2 e^{\frac{1}{\phi_{11}P_1}}}{\phi_{11}P_1} \times \left[Ei\left(-\left(1+\delta_1^u\right)h\left(\delta_2^u\right)\right) - Ei\left(-\left(1+\delta_1^l\right)h\left(\delta_2^u\right)\right) - Ei\left(-\left(1+\delta_1^u\right)h\left(\delta_2^l\right)\right) + Ei\left(-\left(1+\delta_1^l\right)h\left(\delta_2^l\right)\right)\right]. \quad (115)$$

By making use of I obtained in (112), I_5 specified in (113) is evaluated as follows:

$$I_5 = \int_{\delta_1^l}^{\delta_1^u} I.\beta_{1_G}\gamma_{11}f(\gamma_{11})\,d\gamma_{11},$$
$$= \beta_{1_G}\int_{\delta_1^l}^{\delta_1^u}\gamma_{11}\left(1 + \frac{\beta_{2_G}\phi_{21}P_2}{1+\gamma_{11}}\left(e^{-\frac{\delta_2^u(1+\gamma_{11})}{\phi_{21}P_2}} - e^{-\frac{\delta_2^l(1+\gamma_{11})}{\phi_{21}P_2}}\right)\right)f(\gamma_{11})\,d\gamma_{11},$$
$$= \underbrace{\beta_{1_G}\int_{\delta_1^l}^{\delta_1^u}\gamma_{11}f(\gamma_{11})\,d\gamma_{11}}_{\triangleq I_6} + \underbrace{\beta_{1_G}\beta_{2_G}\phi_{21}P_2\int_{\delta_1^l}^{\delta_1^u}\frac{\gamma_{11}e^{-\frac{\delta_2^u(1+\gamma_{11})}{\phi_{21}P_2}}}{(1+\gamma_{11})}f(\gamma_{11})\,d\gamma_{11}}_{\triangleq I_7}$$
$$\underbrace{-\beta_{1_G}\beta_{2_G}\phi_{21}P_2\int_{\delta_1^l}^{\delta_1^u}\frac{\gamma_{11}}{(1+\gamma_{11})}e^{-\frac{\delta_2^l(1+\gamma_{11})}{\phi_{21}P_2}}f(\gamma_{11})d\gamma_{11},}_{\triangleq I_8} \quad (116)$$
$$= I_6 + I_7 - I_8. \quad (117)$$

From (113) and (117), $E[\epsilon_{21}\epsilon_{11_G}]$ reduces to the following:

$$\overline{\epsilon_{21}\epsilon_{11_G}} = I_3 + I_4 - I_6 - I_7 + I_8. \quad (118)$$

In the above equation, I_3 and I_4 are evaluated in (114) and (115), respectively. It is required to evaluate I_6, I_7 and I_8, which are given below. By making use of $f(\gamma_{11})$ obtained in (62), I_6 in (117) is evaluated as follows:

$$I_6 = \beta_{1_G}\int_{\delta_1^l}^{\delta_1^u}\gamma_{11}f(\gamma_{11})\,d\gamma_{11},$$
$$= \beta_{1_G}\int_{\delta_1^l}^{\delta_1^u}\gamma_{11}\left(\frac{1}{\phi_{11}P_1}e^{\frac{-\gamma_{11}}{\phi_{11}P_1}}\right)d\gamma_{11},$$
$$= \beta_{1_G}\left(\left(\delta_1^l + \phi_{11}P_1\right)e^{-\frac{\delta_1^l}{\phi_{11}P_1}} - \left(\delta_1^u + \phi_{11}P_1\right)e^{-\frac{\delta_1^u}{\phi_{11}P_1}}\right). \quad (119)$$

Using (62), I_7 and I_8 in (117) are evaluated as follows:

$$I_7 = \frac{\beta_{1_G}\beta_{2_G}\phi_{21}P_2}{\phi_{11}P_1}\int_{\delta_1^l}^{\delta_1^u}\frac{\gamma_{11}}{1+\gamma_{11}}e^{-\frac{\delta_2^u(1+\gamma_{11})}{\phi_{21}P_2}}e^{-\frac{\gamma_{11}}{\phi_{11}P_1}}\,d\gamma_{11},$$
$$= \frac{\beta_{1_G}\beta_{2_G}\phi_{21}P_2 e^{-\frac{\delta_2^u}{\phi_{21}P_2}}}{\phi_{11}P_1}\left[\frac{e^{-\delta_1^l h(\delta_2^u)}}{h(\delta_2^u)} - \frac{e^{-\delta_1^u h(\delta_2^u)}}{h(\delta_2^u)} + e^{h(\delta_2^u)}Ei\left(-\left(1+\delta_1^l\right)h\left(\delta_2^u\right)\right) - e^{h(\delta_2^u)}Ei\left(-\left(1+\delta_1^u\right)h\left(\delta_2^u\right)\right)\right]. \quad (120)$$

$$I_8 = \frac{\beta_{1_G}\beta_{2_G}\phi_{21}P_2}{\phi_{11}P_1}\int_{\delta_1^l}^{\delta_1^u}\frac{\gamma_{11}}{(1+\gamma_{11})}e^{-\frac{\delta_2^l(1+\gamma_{11})}{\phi_{21}P_2}}e^{-\frac{\gamma_{11}}{\phi_{11}P_1}}d\gamma_{11},$$
$$= \frac{\beta_{1_G}\beta_{2_G}\phi_{21}P_2 e^{-\frac{\delta_2^l}{\phi_{21}P_2}}}{\phi_{11}P_1}\left[\frac{e^{-\delta_1^l h(\delta_2^l)}}{h(\delta_2^l)} - \frac{e^{-\delta_1^u h(\delta_2^l)}}{h(\delta_2^l)}\right.$$

$$\overline{\epsilon_{21},\epsilon_{11_G}} \approx \int_0^{\delta_1^u} U_G(\gamma_{11})\left(\int_0^{\delta_2^u} U_G(\gamma_{21})f(\gamma_{21}|\gamma_{11})\,d\gamma_{21}\right)f(\gamma_{11})\,d\gamma_{11},$$
$$= \int_0^{\delta_1^u} U_G(\gamma_{11})\left(\underbrace{\int_0^{\delta_2^l} U_G(\gamma_{21})f(\gamma_{21}|\gamma_{11})\,d\gamma_{21}}_{\triangleq I_1} + \underbrace{\int_{\delta_2^l}^{\delta_2^u} U_G(\gamma_{21})f(\gamma_{21}|\gamma_{11})\,d\gamma_{21}}_{\triangleq I_2}\right)f(\gamma_{11})\,d\gamma_{11},$$
$$= \int_0^{\delta_1^u} U_G(\gamma_{11})\underbrace{[I_1 + I_2]}_{\triangleq I}f(\gamma_{11})\,d\gamma_{11}, \quad (108)$$
$$= \int_0^{\delta_1^u} I.U_G(\gamma_{11}).f(\gamma_{11})\,d\gamma_{11}. \quad (109)$$

$$+ e^{h(\delta_2^l)} Ei\left(-\left(1+\delta_1^l\right)h\left(\delta_2^l\right)\right) - e^{h(\delta_2^l)} Ei\left(-\left(1+\delta_1^u\right)h\left(\delta_2^l\right)\right)\Bigg]. \quad (121)$$

By substituting I_3, I_4, I_6, I_7 and I_8 in (118), expression for $\overline{\epsilon_{21}\epsilon_{11_G}}$ as given in (48) is obtained.

REFERENCES

[1] J. D. Kumar, P. Mohapatra, and N. Pappas, "Short packet communication over a two-user Z-interference channel with Rayleigh fading," in *Proc. IEEE Globecom Conf.*, 2022, pp. 4746–4751.

[2] A. Ephremides and B. Hajek, "Information theory and communication networks: An unconsummated union," *IEEE Trans. Inf. Theory*, vol. 44, no. 6, pp. 2416–2434, Oct. 1998.

[3] R. R. Rao and A. Ephremides, "On the stability of interacting queues in a multiple-access system," *IEEE Trans. Inf. Theory*, vol. IT-34, no. 5, pp. 918–930, Sep. 1988.

[4] W. Luo and A. Ephremides, "Stability of N interacting queues in random-access systems," *IEEE Trans. Inf. Theory*, vol. 45, no. 5, pp. 1579–1587, Jul. 1999.

[5] V. Naware, G. Mergen, and L. Tong, "Stability and delay of finite-user slotted ALOHA with multipacket reception," *IEEE Trans. Inf. Theory*, vol. 51, no. 7, pp. 2636–2656, Jul. 2005.

[6] N. Pappas, M. Kountouris, A. Ephremides, and V. Angelakis, "Stable throughput region of the two-user broadcast channel," *IEEE Trans. Commun.*, vol. 66, no. 10, pp. 4611–4621, Oct. 2018.

[7] N. Pappas, M. Kountouris, and A. Ephremides, "The stability region of the two-user interference channel," in *Proc. IEEE Inf. Theory Workshop (ITW)*, 2013, pp. 1–5.

[8] P. Popovski et al., "A perspective on time toward wireless 6G," *Proc. IEEE*, vol. 110, no. 8, pp. 1116–1146, Aug. 2022.

[9] A. Kosta, N. Pappas, and V. Angelakis, "Age of information: A new concept, metric, and tool," *Found. Trends Netw.*, vol. 12, no. 3, pp. 162–259, 2017.

[10] R. D. Yates, Y. Sun, D. R. Brown, S. K. Kaul, E. Modiano, and S. Ulukus, "Age of information: An introduction and survey," *IEEE Sensors J. Sel. Areas Commun.*, vol. 39, no. 5, pp. 1183–1210, May 2021.

[11] N. Pappas, M. A. Abd-Elmagid, H. S. Dhillon, B. Zhou, and W. Saad, *Age of Information: Foundations and Applications*. Cambridge, U.K.: Cambridge Univ. Press, 2023.

[12] M. Hayashi, "Information spectrum approach to second-order coding rate in channel coding," *IEEE Trans. Inf. Theory*, vol. 55, no. 11, pp. 4947–4966, Nov. 2009.

[13] Y. Polyanskiy, H. V. Poor, and S. Verdu, "Channel coding rate in the finite blocklength regime," *IEEE Trans. Inf. Theory*, vol. 56, no. 5, pp. 2307–2359, May 2010.

[14] E. MolavianJazi and J. N. Laneman, "A second-order achievable rate region for Gaussian multi-access channels via a central limit theorem for functions," *IEEE Trans. Inf. Theory*, vol. 61, no. 12, pp. 6719–6733, Dec. 2015.

[15] V. Y. F. Tan and M. Tomamichel, "The third-order term in the normal approximation for the AWGN channel," *IEEE Trans. Inf. Theory*, vol. 61, no. 5, pp. 2430–2438, May 2015.

[16] A. Ünsal and J.-M. Gorce, "The dispersion of superposition coding for Gaussian broadcast channels," in *Proc. IEEE Inf. Theory Workshop (ITW)*, 2017, pp. 414–418.

[17] S.-Q. Le, V. Y. F. Tan, and M. Motani, "A case where interference does not affect the channel dispersion," *IEEE Trans. Inf. Theory*, vol. 61, no. 5, pp. 2439–2453, May 2015.

[18] V. Y. F. Tan and A. Roth, "Asymptotic estimates in information theory with non-vanishing error probabilities," *Found. Trends Commun. Inf. Theory*, vol. 11, nos. 1–2, pp. 1–184, 2014.

[19] P. Mary, J.-M. Gorce, A. Unsal, and H. V. Poor, "Finite blocklength information theory: What is the practical impact on wireless communications?" in *Proc. IEEE Globecom Workshops (GC Wkshps)*, 2016, pp. 1–6.

[20] Y. Yu, H. Chen, Y. Li, Z. Ding, and B. Vucetic, "On the performance of non-orthogonal multiple access in short-packet communications," *IEEE Commun. Lett.*, vol. 22, no. 3, pp. 590–593, Mar. 2018.

[21] J. Zheng, Q. Zhang, and J. Qin, "Average block error rate of downlink NOMA short-packet communication systems in Nakagami- *m* fading channels," *IEEE Commun. Lett.*, vol. 23, no. 10, pp. 1712–1716, Oct. 2019.

[22] A. Agarwal, A. K. Jagannatham, and L. Hanzo, "Finite blocklength non-orthogonal cooperative communication relying on swipt-enabled energy harvesting relays," *IEEE Trans. Commun.*, vol. 68, no. 6, pp. 3326–3341, Jun. 2020.

[23] T.-H. Vu, T.-V. Nguyen, T.-T. Nguyen, V. N. Q. Bao, and S. Kim, "Short-packet communications in NOMA-CDRT IoT networks with cochannel interference and imperfect SIC," *IEEE Trans. Veh. Technol.*, vol. 71, no. 5, pp. 5552–5557, May 2022.

[24] X. Sun, S. Yan, N. Yang, Z. Ding, C. Shen, and Z. Zhong, "Short-packet downlink transmission with non-orthogonal multiple access," *IEEE Trans. Wireless Commun.*, vol. 17, no. 7, pp. 4550–4564, Jul. 2018.

[25] J. Choi, "Opportunistic NOMA for uplink short-message delivery with a delay constraint," *IEEE Trans. Wireless Commun.*, vol. 19, no. 6, pp. 3727–3737, Jun. 2020.

[26] U. Somalatha and P. Mohapatra, "Short packet communication over 2-user non-orthogonal multiple access channel with confidential message," in *Proc. Natl. Conf. Commun. (NCC)*, 2023, pp. 1–6.

[27] U. Somalatha, P. Mohapatra, and N. Pappas, "Performance analysis of the wiretap channel with a friendly jammer under finite blocklength," in *Proc. IEEE Globecom Workshops (GC Wkshps)*, 2022, pp. 239–244.

[28] R. H. Etkin, D. N. C. Tse, and H. Wang, "Gaussian interference channel capacity to within one bit," *IEEE Trans. Inf. Theory*, vol. 54, no. 12, pp. 5534–5562, Dec. 2008.

[29] S. Schiessl, M. Skoglund, and J. Gross, "NOMA in the uplink: Delay analysis with imperfect CSI and finite-length coding," *IEEE Trans. Wireless Commun.*, vol. 19, no. 6, pp. 3879–3893, Jun. 2020.

[30] C. K. Kourtellaris, C. Psomas, and I. Krikidis, "Finite blocklength analysis of multiple access channels with/without cooperation," *IEEE Trans. Commun.*, vol. 68, no. 10, pp. 6317–6330, Oct. 2020.

[31] D.-D. Tran, S. K. Sharma, S. Chatzinotas, I. Woungang, and B. Ottersten, "Short-packet communications for MIMO NOMA systems over Nakagami-*m* fading: BLER and minimum blocklength analysis," *IEEE Trans. Veh. Technol.*, vol. 70, no. 4, pp. 3583–3598, Apr. 2021.

[32] X. Lai, Q. Zhang, and J. Qin, "Cooperative NOMA short-packet communications in flat Rayleigh fading channels," *IEEE Trans. Veh. Technol.*, vol. 68, no. 6, pp. 6182–6186, Jun. 2019.

[33] R. Fu, Q. Qi, C. Zhong, X. Chen, and Z. Zhang, "Block error rate analysis of short-packet NOMA Communications with imperfect SIC," in *Proc. IEEE/CIC Int. Conf. Commun. China (ICCC)*, 2020, pp. 68–73.

[34] E. Kurniawan and S. Sun, "Improper Gaussian signaling scheme for the Z-interference channel," *IEEE Trans. Wireless Commun.*, vol. 14, no. 7, pp. 3912–3923, Jul. 2015.

[35] P. Mohapatra, C. R. Murthy, and J. Lee, "On the secrecy capacity region of the two-user symmetric Z interference channel with unidirectional transmitter cooperation," *IEEE Trans. Inf. Forensics Security*, vol. 12, no. 3, pp. 572–587, Mar. 2017.

[36] B. Makki, T. Svensson, and M. Zorzi, "Finite block-length analysis of the incremental redundancy HARQ," *IEEE Wireless Commun. Letters*, vol. 3, no. 5, pp. 529–532, Oct. 2014.

[37] W. Yang, G. Durisi, T. Koch, and Y. Polyanskiy, "Quasi-static SIMO fading channels at finite blocklength," in *Proc. IEEE Int. Symp. Inf. Theory*, 2013, pp. 1531–1535.

[38] W. Yang, G. Durisi, T. Koch, and Y. Polyanskiy, "Quasi-static multiple-antenna fading channels at finite blocklength," *IEEE Trans. Inf. Theory*, vol. 60, no. 7, pp. 4232–4265, Jul. 2014.

[39] J. Scarlett, V. Y. F. Tan, and G. Durisi, "The dispersion of nearest-neighbor decoding for additive non-Gaussian channels," *IEEE Trans. Inf. Theory*, vol. 63, no. 1, pp. 81–92, Jan. 2017.

[40] A. Amraoui, S. Dusad, and R. Urbanke, "Achieving general points in the 2-user Gaussian MAC without time-sharing or rate-splitting by means of iterative coding," in *Proc. IEEE Int. Symp. Inf. Theory*, 2002, p. 334.

[41] G. Kramer, "Topics in multi-user information theory," *Found. Trends Commun. Inf. Theory*, vol. 4, nos. 4–5, pp. 265–444, 2008.

[42] E. MolavianJazi, "A unified approach to Gaussian channels with finite blocklength," Ph.D. dissertation, Dept. Elect. Eng., Univ. Notre Dame, Notre Dame, IN, USA, 2014.

[43] S. Allipuram, P. Mohapatra, N. Pappas, S. Parmar, and S. Chakrabarti, "Performance analysis of a MIMO system with bursty traffic in the presence of energy harvesting jammer," *IEEE Trans. Green Commun. Netw.*, vol. 6, no. 2, pp. 1157–1172, Jun. 2022.
[44] A. Kosta, N. Pappas, A. Ephremides, and V. Angelakis, "Age of information performance of multiaccess strategies with packet management," *J. Commun. Netw.*, vol. 21, no. 3, pp. 244–255, Jun. 2019.
[45] M. Salimnejad and N. Pappas, "On the age of information in a two-user multiple access setup," *Entropy*, vol. 24, no. 4, p. 542, 2022.
[46] H.-M. Wang, Q. Yang, Z. Ding, and H. V. Poor, "Secure short-packet communications for mission-critical IoT applications," *IEEE Trans. Wireless Commun.*, vol. 18, no. 5, pp. 2565–2578, May 2019.

J. DEERAJ KUMAR received the B.Tech. degree in electronics and communication engineering from Sree Vidyanikethan Engineering College, Tirupati, India, and the M.Tech. degree in digital electronics and communication systems from Jawaharlal Nehru Technological University Anantapur, India, in 2017 and 2019, respectively. He is currently a Research Scholar with the Department of Electrical Engineering, Indian Institute of Technology Tirupati, India. His research interests broadly include the areas of finite block-length information theory, its application in short-packet communication, and union of physical layer and network layer.

PARTHAJIT MOHAPATRA (Member, IEEE) received the B.E. degree in electronics and communication engineering from the Biju Patnaik University of Technology, Odisha, India, in 2003, the M.Tech. degree in electronic systems and communications from the National Institute of Technology, Rourkela, India, in 2006, and the Ph.D. degree in electrical communication engineering from the Indian Institute of Science, Bengaluru, India, in 2015. He was working as a Postdoctoral Research Fellow with the iTrust Center for Research in Cyber Security, Singapore University of Technology and Design, Singapore, from March 2015 to July 2016. He was working as an Assistant Professor with the G. S. Sanyal School of Telecommunications, Indian Institute of Technology Kharagpur, Kharagpur, India, from August 2016 to July 2018. Since July 2018, he has been working as an Assistant Professor with the Department of Electrical Engineering, Indian Institute of Technology Tirupati. His primary research interest lies in the broad area of wireless communication and signal processing for communication. His current research interests are in the areas of physical-layer secrecy, finite block-length information theory and its applications to wireless communication, and union of physical and network layer.

NIKOLAOS PAPPAS (Senior Member, IEEE) received the first B.Sc. degree in computer science, the second B.Sc. degree in mathematics, the M.Sc. degree in computer science, and the Ph.D. degree in computer science from the University of Crete, Greece, in 2005, 2012, 2007, and 2012, respectively. From 2005 to 2012, he was a Graduate Research Assistant with the Telecommunications and Networks Laboratory, Institute of Computer Science, Foundation for Research and Technology—Hellas, Heraklion, Greece, and a Visiting Scholar with the Institute of Systems Research, University of Maryland at College Park, College Park, MD, USA. From 2012 to 2014, he was a Postdoctoral Researcher with the Department of Telecommunications, CentraleSupélec, Gif-sur-Yvette, France. He is currently an Associate Professor with the Department of Computer and Information Science, Linköping University, Linköping, Sweden. His main research interests include the field of wireless communication networks with an emphasis on semantics-aware communications, energy harvesting networks, network-level cooperation, age of information, and stochastic geometry. He has served as the Symposium Co-Chair for the IEEE International Conference on Communications in 2022 and the IEEE Wireless Communications and Networking Conference in 2022. He is an Area Editor of the IEEE OPEN JOURNAL OF THE COMMUNICATIONS SOCIETY and an Expert Editor for invited papers of the IEEE COMMUNICATIONS LETTERS. He is an Editor of the IEEE TRANSACTIONS ON MACHINE LEARNING IN COMMUNICATIONS AND NETWORKING and the IEEE/KICS JOURNAL OF COMMUNICATIONS AND NETWORKS. He is a Guest Editor of the IEEE NETWORK on "Tactile Internet for a Cyber-Physical Continuum," and the *IEEE Internet of Things Magazine* on "Task-Oriented Communications and Networking for the Internet of Things." He has served as an Editor of the IEEE COMMUNICATIONS LETTERS and the IEEE TRANSACTIONS ON COMMUNICATIONS. He was a Guest Editor of the IEEE INTERNET OF THINGS JOURNAL on "Age of Information and Data Semantics for Sensing, Communication and Control Co-Design in IoT."